Detecting and Identifying the Lumbar Spine Deformities using Deep Neural Networks

Author

Malaika Mushtaq

321049

Supervisor

Dr. Muhammad Usman Akram

DEPARTMENT OF COMPUTER ENGINEERING

COLLEGE OF ELECTRICAL & MECHANICAL ENGINEERING

NATIONAL UNIVERSITY OF SCIENCES AND TECHNOLOGY

ISLAMABAD

OCTOBER, 2021

Detecting and Identifying the Lumbar Spine Deformities using Deep Neural Networks

Author

Malaika Mushtaq

000000321049

A thesis submitted in partial fulfillment of the requirements for the degree of

MS Computer Engineering

Thesis Supervisor

Dr. Muhammad Usman Akram

Thesis Supervisor's Signature: _____

DEPARTMENT OF COMPUTER ENGINEERING

COLLEGE OF ELECTRICAL & MECHANICAL ENGINEERING

NATIONAL UNIVERSITY OF SCIENCES AND TECHNOLOGY, ISLAMABAD

OCTOBER, 2021

Declaration

I certify that this research work titled "*Detecting and identifying the Lumbar Spine Deformities using Deep Neural Networks"* is my own work. The work has not been presented elsewhere for assessment. The material that has been used from other sources it has been properly acknowledged / referred.

Signature of Student

Malaika Mushtaq

000000321049

Language Correctness Certificate

This thesis has been read by an English expert and is free of typing, syntax, semantic, grammatical and spelling mistakes. Thesis is also according to the format given by the university.

Signature of Student
Malaika Mushtaq
000000321049

Signature of Supervisor
Dr.Muhammad Usman Akram

Copyright Statement

Acknowledgements

All praise and glory to Almighty Allah (the most glorified, the most high) who gave me the courage, patience, knowledge and ability to carry out this work and to persevere and complete it satisfactorily. Undoubtedly, HE eased my way and without HIS blessings I can achieve nothing.

I would like to express my sincere gratitude to my advisor Dr. Muhammad Usman Akram for boosting my morale and for his continual assistance, motivation, dedication and invaluable guidance in my quest for knowledge. I am blessed to have such a co-operative advisor and kind mentor for my research.

Along with my advisor, I would like to acknowledge my entire thesis committee: Dr. Arslan Shaukat and Dr. Farhan Hussain for their cooperation and prudent suggestions.

My acknowledgement would be incomplete without thanking the biggest source of my strength, my family. I am profusely thankful to my beloved parents who raised me when I was not capable of walking and continued to support me throughout in every department of my life and my loving siblings who were with me through my thick and thin.

Finally, I would like to express my gratitude to all my friends and the individuals who have encouraged and supported me through this entire period.

Dedicated to my exceptional parents: ***Mushtaq Hussain & Parveen Nasima****, and adored siblings and friends whose tremendous support and cooperation led me to this accomplishment*

Abstract

Lumbar Spine plays a very important role in our load transfer and mobility. Vertebrae localization and segmentation are useful in detecting spinal deformities and fractures. Understanding of automated medical image is of main importance that will help the doctors in handling the time consuming manual or semi manual diagnosis. Our thesis presents the methods, that will help the clinicians to grade the severity of the disease with confidence, as the current manual diagnoses by different doctors has dissimilarity and variations in the analysis of diseases. In this research we are discussing the lumbar spine localization and segmentation which help for the analysis of lumbar spine deformities. Lumber Spine is localized using YOLOv5 which is the fifth variant of YOLO family. It is the fastest and the lightest weight object detector. Mean Average Precision (mAP) of 0.975 is achieved by YOLOv5. To diagnose the Lumbar Lordosis, we have correlated the angles with region area that is computed from the YOLOv5 centroids and got 74.5% accuracy. Cropped images from YOLOv5 bounding boxes are passed through Hed U-Net which is combination of segmentation and edge detection frameworks, to get the segmented vertebrae and its edges. Lumbar Lordortic Angles (LLA) and Lumbosacral Angles (LSA) are found after detecting the corners of vertebrae using Harris Corner Detector with a very less mean error of 0.29˚ and 0.38˚ respectively. Lumbar spine is segmented using three deep neural models, the best results are achieved by U-Net with highest dice coefficient score (DC) and Intersection over Union (IOU). This thesis compares the results of three deep learning models that are Fully Convolutional framework, U-Net and SegNet architecture.

Key Words: *Deep Learning, Localization, Lumbar Lordortic Angle, Lumbosacral Angle, Lumbar Spine, Edge Based Segmentation*

Table of Contents

List of Figures

List of Tables

CHAPTER 1: INTRODUCTION

Artificial Intelligence (AI) in medical imaging has been very popular from past few years and it helps the clinicians and doctors to diagnose various diseases. Roads accidents are the main cause of spinal injuries due to increasing rate of auto and motor vehicles. As the number of medical images are increasing exponentially, it becomes difficult for clinicians to diagnose with same efficacy and accuracy, but AI has changed the way people used to process large amount of data [1]. Diagnosing the deformity is laborious task and clinicians requires manual methods or Computer Assisted Diagnoses (CAD) tools, which act as a brain of doctors and it have improvise the clinical identification which is less prone to errors. CAD tools support the decision of the radiologists to diagnose the disease efficiently, help in designing the better methods of treatment by finding the pattern of traumatic spinal injuries and to detect the spinal abnormalities using machine learning without human involvement. This research presents the fully automated system to diagnose the lumbar spine deformities such as sway back, flat back and normal lordosis from Magnetic Resonance Imaging (MRI) scans using different machine learning techniques.

1.1 Motivation

60 to 80 % are effected from backache in their lifetime, which is the 5th most common cause for doctor's visit. In 2013 World Health Organization (WHO) presented key facts regarding spinal injuries and deformities that every year almost 250,000 to 500,000 people suffer from spine issues. According to 2016 American journal of public health after stroke spine issues are the second leading cause of paralysis. Magnetic resonance imaging (MRI) and computed tomography (CT) technologies are used to detect various spinal disorders by Machine Learning (ML) techniques which assist the surgeons and physicians to diagnose the disease without going into time-consuming manual methods. Timely diagnoses of spine deformities can prevent the patient from dangerous consequences and help in treating the disease at its early stage. There are very less chances of finding an expert doctor or radiologists in the rural area of Pakistan, the motivation for this research is to detect the spinal deformities and act as a vote of confidence for young radiologists.

1.2 Problem Statement

Timely diagnosis of spinal injuries can help to prevent from the lifetime paralysis. Many systems have been proposed to locate and segment the spine and detect the deformities, but due low accuracy and speed, desired results are unable to obtain. The main purpose of this research is to develop a fully automated system using machine learning and deep learning techniques with improved accuracies that will support the clinician's manual diagnosis of lumbar spine diseases.

1.3 Aims and Objectives

Major aims and objectives of this research can be written as:

- To provide the annotated dataset to research community.
- To develop object detection framework for lumbar deformities.
- To implement the simple architecture neural network which is faster than the conventional neural networks.
- To segment the lumbar vertebrae and sacrum precisely using machine learning techniques.
- To develop the diagnostic system for grading the severity of lumbar deformity.

1.4 Structure of Thesis

This structure of the thesis is as follows:

Chapter 2 describes the spinal structure and its connection with brain. It also covers the spinal pathologies and its effect on human body.
Chapter 3 discusses related work and the models used for vertebrae identification and localization and different datasets used by research community to diagnose spinal diseases.
Chapter 4 covers the detailed methodology that includes two parts, the first part is the localization of lumbar vertebra and sacrum followed by the segmentation.
Chapter 5 discusses the dataset used for analysis. Results are reported with all tables and figures in details.
Chapter 6 concludes the work done and discloses some of the future work that can be done in this research

CHAPTER 2: SPINE AND MRI SCAN

Spinal Cord is the second main organ of Central Nervous System (CNS) after brain. CNS acts central processing unit in human anatomy, controlling all the crucial life depending on processes of body. Brain act as a command center while spinal cord is the pathway from where body sends and receives messages from the brain and to the brain. This chapter will covers the spine anatomy, medical imaging techniques, planes of the body, comparison of MRI and CT scans, MRI scan construction and sequences and different spinal deformities.

2.1 Spine Anatomy

Spinal cord is about 40 to 50 centimeter long, it's a cluster of tissues and nerves curled together in a twisted manner. Spinal cord acts as a transition hub line of information from brain to the rest of the body. The reflexes control, the mobility of body like twist, turn and bending relay upon spinal code even one can say that the whole skeleton structure is balanced with the support by spine. Spine deformity can occur by birth, due to aging, injury or due to spine surgery. Human spine consists of 26 vertebrae, first seven in the neck are called cervical, twelve in the torso are called thoracic and five in the lower back are called lumbar vertebrae as shown in Figure 2.1.

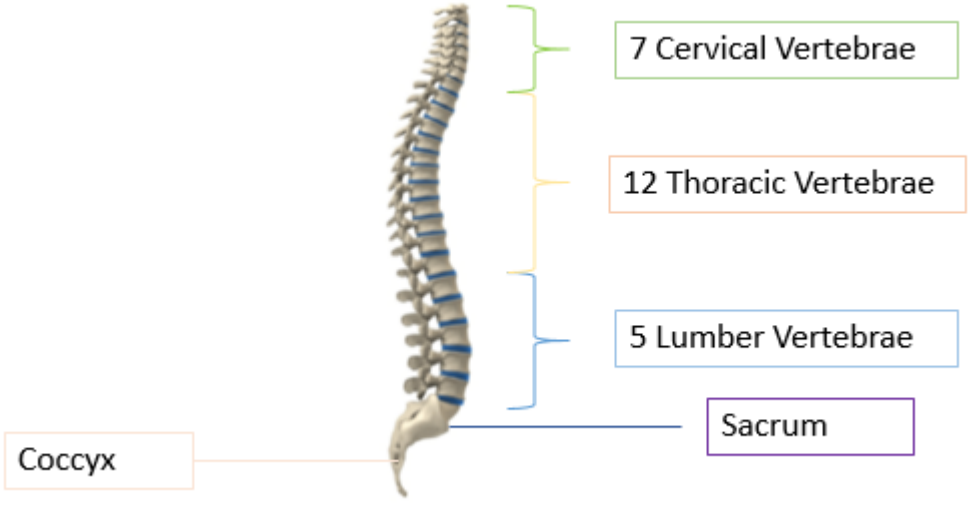

Figure 2.1: Anatomy of Spinal Cord [2]

The other two are fused sacrum and coccyx bone. The lumbar vertebrae numbered from L1-L5, are used to carry the weight of the body and are more prone to deformity. Lumbar starts after the thoracic vertebrae and ends at sacrum bone. Lumbar spine is between the pelvis and the ribcage and is responsible between the communication between the brain and legs.

2.2 Medical Imaging Techniques

Body can be visually represented for medical analysis through medical imaging. Different type of medical imaging includes, X-ray, Magnetic resonance imaging (MRI) and computed tomography (CT) technologies. All these types are used to detect various spinal disorders by Machine Learning (ML) techniques which assist the surgeons and physicians to diagnose the disease without going into time-consuming manual methods. Timely diagnoses of spine deformities can prevent the patient from dangerous consequences and help in treating the disease at its early stage. X-ray only tells about broken bone and not about the muscles issues, MRI scan is good at detecting small herniation of discs, pressed nerves and soft tissue related issues, while CT is more useful in detecting the moderate and high risk spinal fractures and injuries due to its clear bones' structure. Medical Imaging helps doctors in diagnosing the spinal deformity and they can correlate it with pain symptoms. Diagnosing the deformity is laborious task and clinicians requires manual methods or computer assisted diagnoses tools.

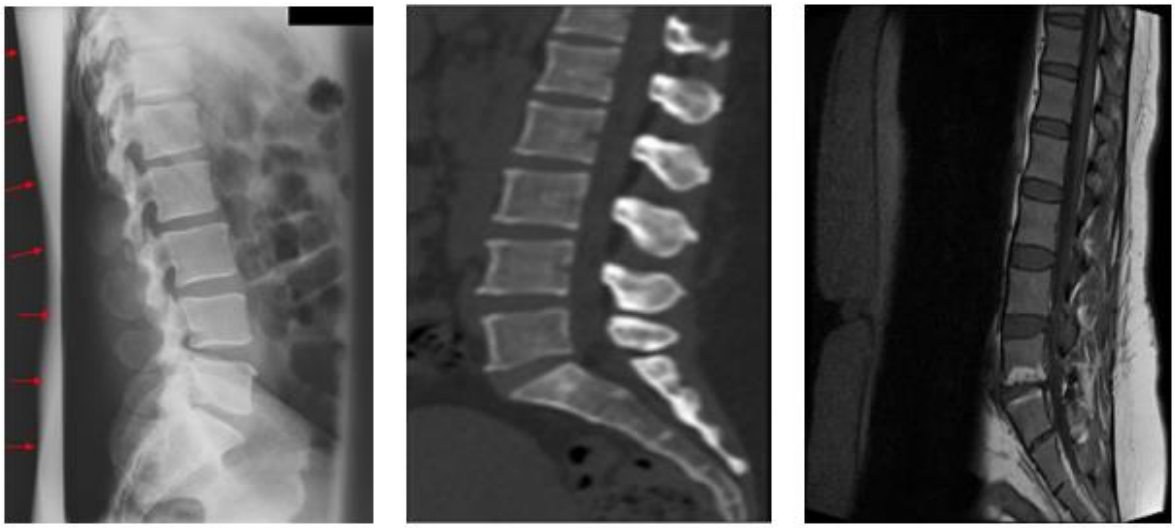

(a) (b) (c)

Figure 2.2: (a), (b) and (c) represent the X-ray, CT and MRI scans of lumbar spine

2.3 Planes of body

It is helpful for the clinician's to view all the planes to get more insight of anatomy and know the extent of pathology. There are normally three planes, which are given below:

1. Axial Plane
2. Coronal Plane
3. Sagittal Plane

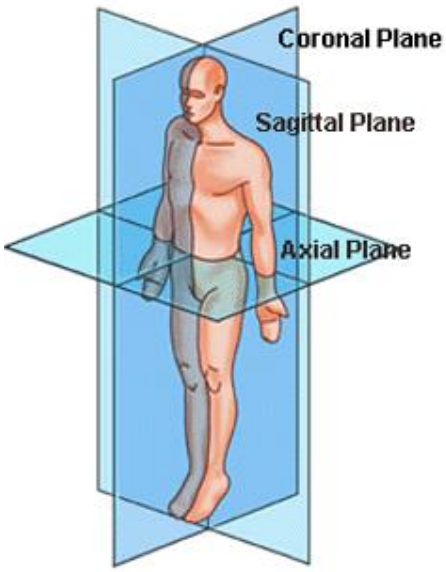

Figure 2.3: Three planes of body [3]

- **Axial Plane**

This plane is parallel to the ground, it separates the body feet from the head as shown in the figure. It is x-y-z plane and its orientation is from the top down. In the coordinate system, x is the axis which goes from back to front, y is from right to left and z is the axis that goes from top to bottom.

- **Coronal Plane**

This plane is perpendicular to the ground, it separates the front of the body to back of the body. It is x-z plane and its basic orientation is from the front.

- **Sagittal Plane**

This plane is also perpendicular to the ground but its plane is x-y and its basic orientation is from side of body. It separates the right from left, where mid-sagittal view is exactly the center of body from the side.

2.4 CT and MR Scans Comparison

Patients feel safe and comfortable taking MRI test as compared to CT test because MRI does not use any kind of radiation while in CT, a patient is exposed to more radiation rather than single X-ray radiation. CT uses X-rays radiation and number of X-rays images taken through different angles to get the image of the body and is more detailed than normal X-ray. MRI produces detailed image by using the radio waves and strong electromagnetic fields. As MRI is more detailed, so for organ or muscles related problems doctor suggest to take MRI scan while for bone related issues CT are more preferred by doctors [4]. MRI scan can investigate usefully the lower back pain, MRI test sequence and MRI details will also be discussed. The Figure show the MRI and CT of lumbar spine.

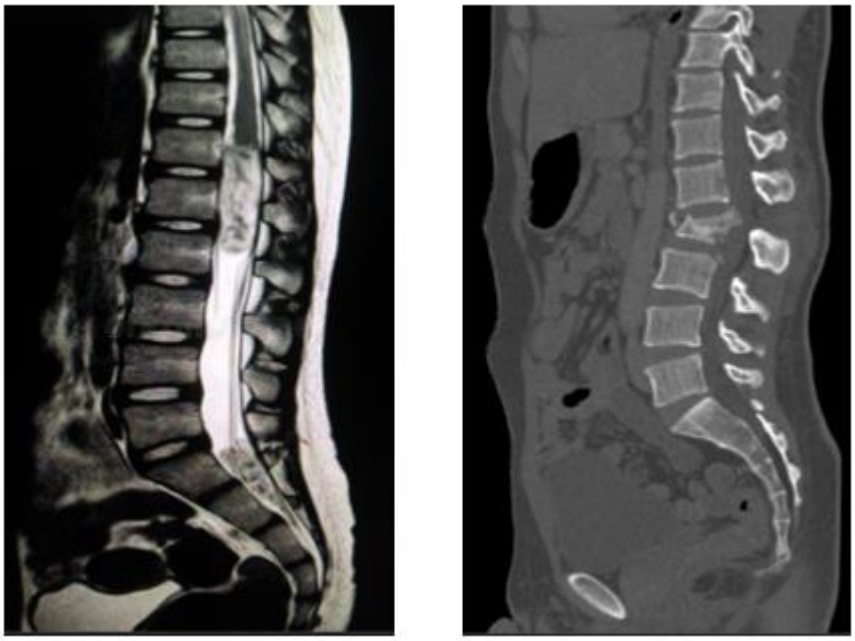

(a) (b)

Figure 2.4: MRI and CT scan of spine.

2.5 MRI Image Construction

MRI measures the water present in the tissues of the body and shows the location of water in the body by using radio waves and strong electromagnetic field, this information is used to produce a detailed image. MRI magnetic field is much stronger than the magnetic field of earth [5]. Our body has up to 65 percent of water and water is made up of hydrogen and oxygen. Hydrogen has interesting impact on MRI, because its nucleus act as tiny magnet when in isolation. The process is called precession as these tiny magnets align with external

field when body is exposed to magnetic field. The radio frequency excites the hydrogen nuclei containing protons. As soon as the radio frequency is turned off, it de-excites the protons and they generates the MR signal which constructs the image by making use of spatial encoding [6][7].

Tissues can be group by different relaxation time, T1 relaxation and T2 relaxation [8]. Mostly T1 weighted and T2 weighted images are generated in axial and sagittal views [9]. It can be seen from the figure that T1-weighted images represents fat structures as white (bright) which shows the high intensity signal while T2 weighted represents fluid and fat based as white (bright). T1 are suitable for anatomical representation while T2 weighted images are suitable for disease evaluation. [10]

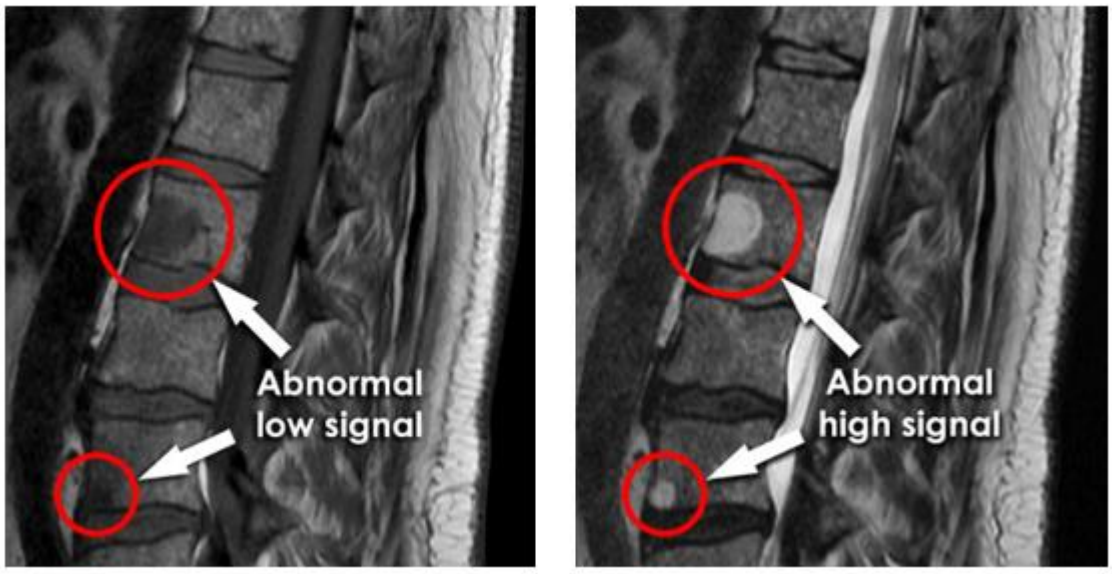

(a) (b)

Figure 2.5: (a) and (b) represents T1 and T2 weighted images [10].

2.6 MRI scan Sequence

As obvious from the previous discussions, MRI scan is suitable to inspect the lower back pain. A patient is asked to undergo the MRI scan to investigate the actual reason behind the lower back. MRI usually takes 30 to 60 or up to 2 hours [11] depending upon the machine's magnetic field. In most of the cases only axial and sagittal slices are generation, but for some cases coronal slices can also be generated. When the MRI scan is completed, radiologist get the Digital Imaging and Communications in Medicine (DICOM) [12] images through Picture Archiving and Communications System (PACS) [13]. Radiologist do not examine the patient physically, after seeing the MRI scans it reports the findings only. Patient takes MRI scans and radiologist report to referred consultant, who gives the final verdict after evaluating the

patient clinically and correlating the reports with the pain symptoms. The decision is then made to treat the disease by invasive or noninvasive procedures.

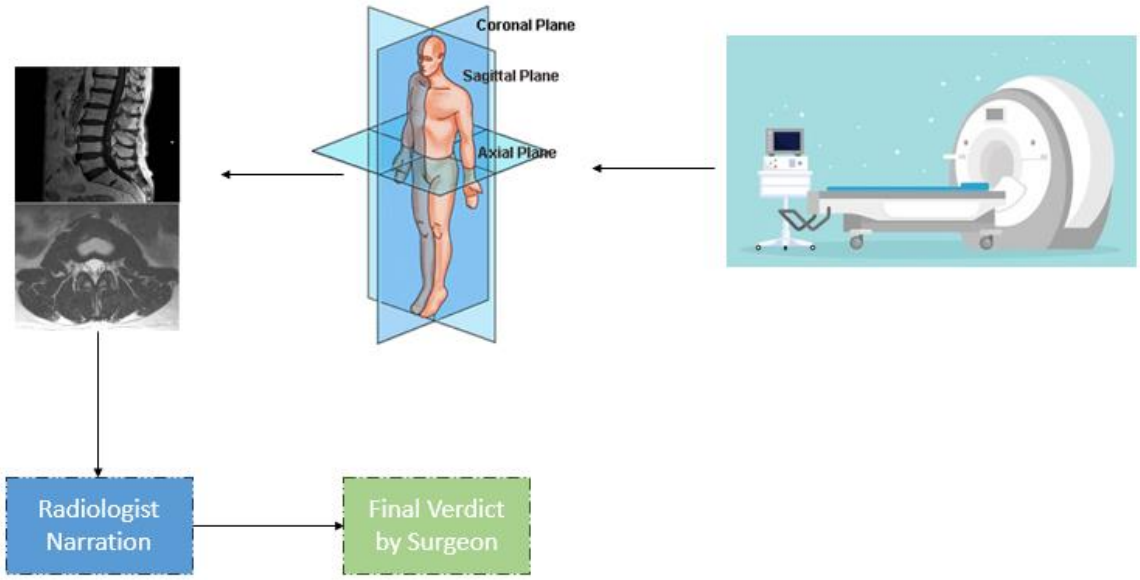

Figure 2.6: MRI scan sequence

2.7 Spine Deformities

Backache have mild to serious pain symptoms which affect the daily life. Heavy mechanical stress causes the slip of disc in the L4 to L5 region or L5 to S1 region. Deviation from the normal lumbar curve results into lumbar spine deformities. As we know, sagittal plane divides left from the right we will be working on the mid sagittal images in this thesis. Degenerative changes are occurring in the spine due to various factors that affect the postures of the body as shown in figure 2.7.

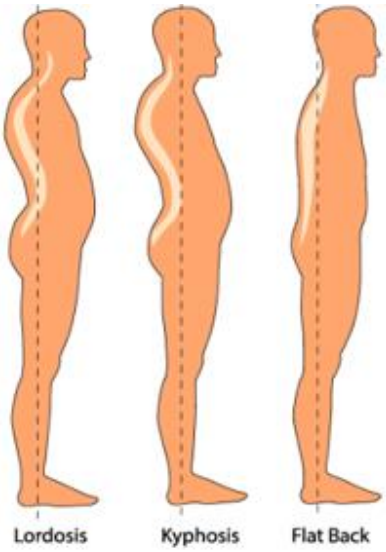

Figure 2.7: Different Spine Deformities

Sagittal Lumbar spine has various deformities, some of them are:

1. Lordosis
2. Kyphosis
3. Flat Back Syndrome

Lordosis

Normal lumbar spine has an inward curve known as lordosis. Normal lordosis is not painful but if the curve is abnormally inward it will affect the posture of a person and he will experience pain. Curve of lumbar spine determines the deformity, doctor recommends different treatment depending on the type of lordosis, curve may be sway back or flat back. If the Cobb angles are less the normal range it is termed as hypo lordosis while if the angle is greater than normal range of lordosis it is called hypo lordosis.

Causes

Lordosis can be caused from various reasons, according to [14] following are the causes of lordosis:

Obesity

Obesity causes the curve to deviate from normal position, it also causes other diseases like heart problems, diabetes and cancer.

Osteoporosis

It is the disease that decreases the bone strength and patient is more prone to sudden bone fracture.

Spondylolisthesis

In Spondylolisthesis, one of the vertebra slips on the vertebra below it. It can be treatable without the surgical intervention depending on the severity of the disease.

Achondroplasia

It is the bone growth disorder which is often in dwarfs.

Osteosarcoma

It is the bone cancer and often arises in adults of age below 20 due to an active growing center of bone.

Symptoms

Most common type of lumbar lordosis is the muscle pain, because as the curve changes the muscle become tighten causing pain. Other symptoms includes:

- Difficult to maintain the muscle control
- Numbness
- Weakness
- Tingling
- Low bladder control

Diagnoses

Lordosis can be diagnosed by many ways, one way is to lay on the flat floor and check the space between the curve and floor and your back and neck. If your hand slide easily through this space than you have lordosis. Doctor will examine the lordosis by making the patient bend to the side and forward. He checks whether the curve is flexible, the movement of spine, spine alignment, and check for any other abnormalities. After examining the doctor will refer the MRI and other tests to determine lordosis by analyzing the angle based on your age, height, and weight.

Treatment

Doctors chose the treatment based upon the severity of the curve and other symptoms. Treatment that can cure the lordosis includes:

- Medicines for reducing the swelling and pain.
- Overcome obesity
- Daily exercises and physical therapy
- Surgery for the most severe cases

Kyphosis

Kyphosis causes the upper back of the body to bend forward abnormally. It is most common in old women, but any age group can be affected from kyphosis. Poor posture of the body, weakness due to age and spine abnormalities results in kyphosis. It causes discomfort and severe pain depending on the type of the curvature.

Causes

Spine contains vertebrae which are stacked upon each other, which allows the spine to be flexible and supportive to the body. Kyphosis occurs in the thoracic region, which is the upper part of the spine. The shape of this region become wedged and curve bends more than usual in the forward direction. Its causes includes:

- Old age
- Bad posture
- Abnormalities in the shape of vertebrae
- Development of abnormal patterns

Symptoms

The main symptoms of kyphosis is the bending of upper back in an abnormal manner. The upper back is hunched over and shoulders are bended round in forward direction. Kyphosis may or may not cause any symptoms, in mild cases it shows no signs. According to [15] below are the symptoms for kyphosis:

- Back Ache
- Bended forward back
- Stiffness in thoracic region
- Inflexibility in hamstrings

Diagnoses

Doctors diagnose kyphosis through medical history of the patient and physical exercises. A very common test is examining of the spine while patient is laying on the flat surface. It is due to the poor posture if it straights out which shows spine is still flexible. If it does not straights out then it may be due to other reasons. The doctor can take x-ray of the patient to look in to its structure or can take the blood test in most severe cases.

Treatment

Treatment of kyphosis varies from severity to mildness. Doctor will diagnose the severity through different methods as discussed earlier. Treatment may be surgical or nonsurgical. Cases that are not very severe can be treated without surgical intervention. Nonsurgical treatment includes various physical exercises which reduce the spine pressure and discomfort and improve the posture of the body. If spine is in growing phase then the doctors recommends spinal brace which helps in correcting the posture of the body. Surgical treatment includes spinal fusion or welding of more than two vertebrae to form a single bone. Other surgical methods including inserting plates and rods into the spine to correct the posture of the body.

Flat Back Syndrome

Spine is made of four natural curves, two of them are lordotic curve while other two are kyphotic curve. All these natural curves balances each other and form S shape in spine. When the lower curvature becomes flat during the period of time then it is called flat back syndrome. Lordosis is decreases in this syndrome and posture of the body becomes bend forward. Symptoms may not be felt at first but as time passes it becomes worst and patient back bends further.

Causes

Flat Back syndrome occurs when there is decrease in the lordosis. According to [16], following can cause the flat back syndrome:

Degenerative disc

Spine is made up of vertebrae and discs. Disc acts as the shock absorber and soft tissue cushion making the spine flexible. As the age increase, disc starts degenerating which in turn decreases the lordosis making the spine bend forward. This act as a contribution to flat back syndrome and patient may feel discomfort and pain due to imbalance in spine and degenerative disc.

Vertebral Compression Fracture

This often occurs due to the osteoporosis where bone strength has weaken and patient is more prone to bone fracture. It can cause the height loss of spine and fracture may be in one or more bones which changes the alignment and structure of the spine resulting into flat back syndrome.

Ankylosing Spondylitis

It is the inflammatory disease which affect the spine chronically. As the time passes it causes arthritis, stiffness and restabilization of spinal vertebral bodies causing the bend forward posture.

Lumbar Post Laminectomy Syndrome

Flat back syndrome occurs in patients who have previously undergone through laminectomy or other treatments to treat stenosis. This can cause the spinal instability and decrease the lumbar lordosis.

Symptoms

Symptoms may not be shown in the start but as time passes different symptoms appears deforming the posture of the body. Others symptoms includes:

- Leg pain
- Muscular fatigue
- Back pain
- Bend forward posture over time

Diagnosis

Flat back syndrome can be diagnosed from medical history of patient, physical exercises, physical examination and through radiography. Doctors visualize the radiography results to analyze the tilt in the spine, MRI or CT do not diagnose this syndrome but can identify other deformities like spinal stenosis which may be affected due to changing alignment of spine. Physical exam is necessary to diagnose flat back where doctor examine the posture of body like changes in pelvic tilt and flexibility of hips and knees.

Treatment

Flat back can be treated by invasive and non-invasive procedures. Non-invasive procedures for treating the flat back syndrome include daily exercises like aerobics, strengthening of core muscles, weight lifting. This will help the patient to relieve pain and also help to strengthen the bones. In worsen pain cases like pinched nerve, an injection can be prescribed to reduce the pain of the patient. Non-invasive procedures can treat the patient symptoms if not worsen over time without the surgery. Surgeons recommends invasive procedures after going through detailed review of MRI and CT scans. Invasive methods to treat the flat back syndrome includes combine or multiple techniques.

Different spine diseases with their symptoms, diagnoses and treatment have been discussed which can cause lifetime paralysis if not cured early. Different imaging tests are used to get the insight of anatomy and know the extent of the pathology. MR scan is more appropriate for organ and muscles related issues and a patient is asked to go under the MR scan to get the actual reason of the disease. Three body planes are used to view the anatomy and degree of disease from different planes.

CHAPTER 3: LITERATURE REVIEW

AI is growing vastly in medical imaging and automated systems have been developed by many researchers to diagnose different diseases and help the doctor to choose less invasive surgical procedures. Many researches have been taken on lumbar spine as it is responsible for lower backache. Due to heavy mechanical stress, slip often occurs at L4 to L5 or L5 to S1. In past, many approaches have been applied on the vertebrae to detect, segment and identify various diseases, but still researchers are working on better and new techniques to diagnose the diseases more efficiently.

Many researches have been taken on spinal diseases to timely diagnose the diseases as they have dangerous consequences. CT and MRI scans are used to evaluate particular body parts. The literature is carried out on journals, conference papers and electronic books from recent past. From the past few years, innovative research has been carried out on computer aided diagnosis (CAD) tools to diagnose the spinal diseases in CT and MRI scans. Some of them have developed different segmentation techniques of vertebrae while others are more focused to localize and classify the vertebrae. This chapter will sum up all the researches done in this field.

3.1 Localization

Localization identify the location of the objects in an image and draws a bounding box around the objects. Various experiments have been perform to localize the vertebrae and diagnose the spinal deformities. Some of them are presented in the chronological order.

Lecron et al. [17] have tried to develop an automatic approach to detect the vertebra. The purpose of developing such a model is to detect vertebra without human involvement. They have got the points of interest in radiography by an edge polygonal approximation, and SIFT descriptor is used to train a SVM model. They concludes that their results is very promising with a corner and vertebrae detection accuracy rate upto 90% and 86%. Glocker et al. [18] have developed a novel approach based on a regression tree. They have used two datasets and have a total of 424 CT scans images with different pathologies. Each classification forest is trained to a maximum depth of 24 trees and consists of 20 trees. Their approach works better than Regression Forest+HMM on pathological spine CT. Boundary detection method using dynamic programming is developed in [19]. They have calculated the euclidean distance

between their method of detecting the boundary and manual labelling of lumbar spine and achieved the mean euclidean distance of 3mm. New approach to localize objects is YOLO having different variants to detect the objects. Zuzanna et al. [20] uses YOLO to detect different regions in the pelvic area and they have achieved cumulative precision, recall and accuracy of 99% 99% 98%. James et al. [21] have proposed a system to detect and localize vertebrae. It detects vertebrae using 3D samples and identifies the specific vertebrae using 2D slices. Their results shows very accurate identification and localization of vertebrae. They attained the mean and std of localization error upto 5.60, 7.10. Modified YOLOv3 is developed in [22]. They have used the approach to locate the IVD and detect disc herniation. They have achieved inference time equal to YOLOv3 with less number of parameters.

A disease called Adolescent idiopathic scoliosis (AIS) has been investigated in [23] that often arises in children. To treat scoliosis, correct measurement of Cobb angles can help doctors. They have proposed to first localize the vertebrae center and then detect its landmarks through corner offset. Their results are much better with the mean error value 50.11 which is less than regression and segmentation based methods.

Masuzawa et al. [24] proposes the novel approach to perform localization, segmentation, and identification simultaneously. They have worked on two different datasets, in the first stage, they train a 3D Fully Convolutional Network (FCN), whose task is to localize the thoracic, cervical, and lumbar vertebrae. In the second stage the network takes an auxiliary channel along with the 3D CT images, the output is the next vertebra. The algorithm has achieved a mean dice score of 96%, an error of 8.3mm and identification accuracy of 84%. Gang et al. [25] have proposed a novel approach of adding three CNN layers in YOLO tiny. Their system is used to detect spinal fractures with accuracy 85.63% and IOU upto 87.3. Pisov et al. [26] have worked on a publicly available dataset of chest to detect the early stage of osteoporosis. Another two step algorithm is proposed by them, which is used to localize the vertebral column in 3D CT images and the next step is to detect each vertebrae and look for fractures in 2D. They have trained neural networks for both steps on GPU using an easy 6-keypoints based annotation scheme. Their error is very less up to 1mm with very high accuracy up to 0.99. The summary of literature review of localization is shown in table 1.

Table 1: Literature Review of Localization techniques

Sr. No	***Study***	***Year***	***Technique***	***Dataset***	***Results***
1	Lecron et al. [17]	2012	Multi-Class SVM	250 cervical vertebrae X-Ray Images	corner detection rate 90.4% and vertebra detection rate 81.6% to 86.5%
2	Glocker et al. [18]	2013	dense classification	424 CT scans	70 % overall and 75% lumbar
3	Koh et al. [19]	2014	Dynamic Programming	MRI scans	Mean Euclidean distance 3mm
4	Zuzanna et al. [20]	2018	YOLO	677 CT scans from 4 datasets	Cumulative Precision Recall and Accuracy of 99% 99% 98%
5	James et al. [21]	2019	Two stage CNN	spine CT dataset	Mean and std Localization error 5.60, 7.10
6	Zhong et al. [22]	2019	Modified YOLO	Guanxi College Students Artificial Intelligence Design Competition MRI imaging data	Inference Time 24.3ms and 23.9ms
7	Yi et al. [23]	2020	ResNet34	AASCE MICCAI 2019	Error 50.11
8	Masuzawa et al. [24]	2020	Cascaded Convolutional Neural Networks	MICCAI CSI 2014	mean Dice score of 96%,mean localization error of 8.3 mm, mean identification rate of 84%
9	Gang et al. [25]	2020	Improved Yolo-tiny	spine CT images	mAP (mean Average Precision) 86.63%,IOU ((Intersection Over Union) is 87.3
10	Pisov et al. [26]	2020	U-Net that consists single Region Proposal Network (RPN),	CT images	Precision 0.993

3.2 Segmentation

Segmentation is use to segment different objects in an image. Many researches have been performed to segment the vertebrae and diagnose the diseases and herniation in the discs. Some of them are presented in chronological order.

Ghosh et al. [27] have proposed a system that uses two methods to detect and localize the IVD. They detects IVD by using different machine learning algorithms and segments all the tissues in lumbar sagittal MRI by using different features and trained them on robust classifiers. They have achieved promising results with both methods. To predict the centroids coordinates of vertebrae, a deep network has been deployed in [28]. They have used the public dataset of CT volumetric images and got accuracy up to 90%. Ala S. et al. [29] have developed a system to find the herniation in disc by taking centroid distance function as a shape feature. They concludes that this feature can be visualized as best indicator of disc herniation in MRI scan axial images. A cascaded FCN is developed in [30]. They have trained the 3D FCN to get the lumbar shape and called it a localization Net, and then they have trained another 3D FCN to segment the cropped lumbar and called it a segmentation Net. The localization net has helped the segmentation net to segment the lumbar region correctly. Their results are pretty good with a dice coefficient of 95%. Liao et al. [31] have worked on arbitrary CT images which is a demanding task. As all the images have different shapes and appearances, it is very difficult to segment and localize vertebrae. So, they have solved the problem by working on short-range contextual information and long range contextual information. For short-range contextual information, they have proposed a 3D FCN to extract the features and for long-range contextual information, they have used the bidirectional recurrent neural network to encode the contextual information. They have concluded that their method extracts better feature representation than previously used methods on this challenging dataset with a notable margin. In [32], authors have presented their work at Large Scale Vertebrae Segmentation Challenge (VerSe) in 2019 where they have used human-machine hybrid algorithm, with 95% of high vertebrae identification rate and 90% Dice Coefficient. They have used three steps to identify vertebrae, first step is to detect vertebrae, second step is to label the vertebrae that is based on btrfly architecture and third step is to segment vertebrae that was performed by U-Net.

In [33], researchers have worked to detect the lumbar spinal stenosis (MRI) images. They have worked on axial view of the images and applied SegNet with different training ratios. Vertebrae segmentation and labelling by using a FCN is presented by Nikaolas et al. [34]. They segments the vertebrae by combining the network with a memory component that keeps information about already segmented vertebrae. After segmentation, it then searches for another vertebrae that is located next to the segmented one, and predicts whether it is visible enough to process for further analysis. It has a very high accuracy of 93% with only one mislabeled vertebrae case. Mabarki et al. [35] have worked on Convolutional Neural Networks (CNN) based on VGG19 architecture to detect the herniation in the lumbar disc. They have tested the system successfully with more than 200 patients. Friska et al. [36] have developed an automated system to measure the foraminal widths and anteroposterior diameter to determine the disease called lumbar spinal stenosis. They have used SegNet to get six region of interests in composite axial MRI Images. They have reported 97% agreement with the specialists opinion to identify the severity in the inter-vertebral disc herniation. In [37], authors have worked on the mid sagittal view of the MRI images. They uses two segmentation techniques, the first technique was a customized algorithm and the other was semantic segmentation. They get good results in classification of spondylolisthesis and lumbar lordosis. The main purpose of these researches are to aid the clinicians' in handling the time taking task of manual image labelling. The summary of literature review of segmentation part is shown in table 2.

Table 2: Literature Review of Segmentation techniques

Sr. No	***Study***	***Year***	***Technique***	***Dataset***	***Results***
1	Ghosh et al. [27]	2014	Auto Context Approach for segmentation and robust classifiers for localization	212 MRI images	Segmentation DC of 0.84 and 0.87 for intervertebral disc and dural sac and 98% disc localization accuracy
2	Yang et al. [28]	2017	Deep Image-to-Image Network(DI2IN)	CT scans	Identification rate 90%
3	Ala S. et al. [29]	2017	Manual Segmentation	MRI images	-
4	Janssens et al. [30]	2018	FCN-U-NET	CT scans	DC 95.77 ± 0.81%
5	Liao et al. [31]	2018	CNN+Bi-RNN	CT images	Identification rate 88.3%
6	Sekubayina et al. [32]	2019	FCN-Btrfly architecture-U-Net	Verse 2019 Dataset	95% vertebrae identification rate and 90% Dice Coefficient
7	Ala S. et al. [33]	2019	SegNet	515 MRI Scans	Intersection over union unregistered, intervertebral disc, posterior element, thecal sac,aap,other 0.21,0.92,0.78,0.85,0.53,0.98
8	Lessman et al. [34]	2019	FCN	MRI and CT scans	DC 94.9 ± 2.1%
9	Mbarki et al. [35]	2020	CNN	MRI scans	Accuracy 94%
10	Friska et al. [36]	2020	SegNet	MRI scans	average error left and right foraminal distances 0.29mm, 0.28mm
11	Masood et al. [37]	2021	ResNet-U-Net	MRI scans	DC 0.97

3.3 Different Methods of Cobb Angles

Bagus Adhi Kusuma [38] in his research article has addressed the detection of scoliosis using x-ray images. 3 The author has preprocessed by converting X-ray images to grey scale and marked seed locations that divides image to 12 sub-images. Later median filtering and canny is applied to get the boundary or vertebrae. After center point calculations polynomial curve fitting and cobb angle estimation with help of gradient equation is achieved. K-Mean clustering has played a significant role to determine the scoliosis curve. The procedure average deviation is less than 6 degrees. Yaling Pan et al. in [39] has used two separate Mask

R-CNN models to segment and detect the spinal curve and all vertebral bones on 248 X-rays. The Cobb angle is measured from the output of these models. Measuring the angle between any interior and superior perpendicular of the cranial and caudal vertebrae. A set containing all possible angles is obtained, and a maximum angle is considered as the Cobb angle. To assess the reliability and accuracy two experienced radiologists separately measured the cobb angle manually output results of these models is compared achieving intraclass and interclass correlation coefficients 0.941 and 0.887, respectively. In [40] A. Safari et al. has developed a semi-manual approach for the estimation of cobb angle. Contract stretching is used to extract the ROI in input X-Ray image. The curvature of spine is determined with help of manual landmarking at least one point for each vertebra, 5-th order polynomial curve is fitting is applied. After determining the morphologic curve, the final phase is to estimate the cobb-angle by using tangent equation. The equation is calculated at the inflection points, and the angle is between two perpendicular lines to the spinal curve. The paper claims the correlation coefficient between the angle values is 0.81. In paper [41] a new high-precision regression technique, Adaptive Error Correction Net (AEC-Net) is introduced for evaluation of cobb angle from x-ray images of spine. The proposed technique has 2 modules first one is regressing landmark net for boundary features extraction that indirectly support in cobb angle calculation. The second one is Angle Net for direct approach for cobb calculation using curve features. The final stage is Error correction Net that basically estimates both modules output using extrapolation to identify the difference in cobb angles from both networks. To evaluate the results 581 spinal anterior-posterior x-ray images are utilized attaining Mean Absolute Error 4.90 in cobb angle. Kang Cheol Kim et al in [42] has presented an approach to identify scoliosis from X-rays images, he explained the drawbacks of manual measurements which are laborious and time taking. The method consists of three major parts, in first part confidence map is utilized for localization. In the second part vertebral-tilt field is used for the estimation of slope of each vertebra, and in the third part the Cobb angle is measured using vertebral centroids in combination with the calculated vertebral-tilt field. The performance is evaluated, accomplishing CMAE of 3:51 degree and SMAPE of 7:84% for the Cobb angle. The main purpose of these researches are to aid the clinicians' in handling the time taking task of manual image labelling. The summary of different cobb angles measurement techniques is shown in table 3.

Table 3: Different Techniques to find cobb angles

Sr. No	***Study***	***Year***	***Technique***	***Dataset***	***Results***
1	Bagus Adhi Kusuma [38]	2017	Canny Edge Detection Polynomial Curve Fitting K-Means	28 X-Ray	Average Deviation 5.86 degree
2	Yaling Pan et al.[39]	2019	Faster R-CNN	248 X-Ray	ICC intra 0.941 and inter 0.887 MAD was 2.20° and 2.94
3	A. Safari et al. [40]	2019	Manual Landmarking and Curve fitting Cobb-angle Estimated	14 X-Rays	Correlation Coefficient 0.81
4	Bo Chen et al.[41]	2019	Adaptive Error Correction Net (AEC-Net)	581 X-Ray	Mean Absolute Error 4.90
5	Kang Cheol Kim et al [42]	2020	Centroid-net M-net	481 X-Ray	Circular MAE 3:51 Symmetric MAPE 7:84%

3.4 Datasets

Number of datasets have been developed by hospitals and challenges to diagnose the spinal disease. Some of the re-known publicly and paid datasets are given below:

1. SpineWeb provides numerous resources of CT scans and x-ray radiographs. It has 16 different datasets for different pathologies identification.
    a) Dataset 1: It has 30 pair of CT scans and MRI of same subject.
    b) Dataset 2: It has 10 CT scans of youngsters. The spine is already segmented in this dataset and have thoracic and lumbar region [43].
    c) Dataset 3: CT scans of 125 patients have been provided by Imperial College London and is publicly available for research purposes [18]. This dataset was used as a training dataset in CSI 2014 challenge.
    d) Dataset 4: It contains the dicom and bmp formats of CT scans of five patients [44].
    e) Dataset 5: [45] provided the CT scan of 10 normal person having 5 lumbar vertebrae.
    f) Dataset 6: It contains multi modality MRI images of 8 persons of lower spine from T11 to L5 with seven IVDs .

g) Dataset 7: It contain the 3D T2 weighted Turbo Spin Echo (TSE) MRI images of 15 patients in Neuroimaging Informatics Technology Initiative (NIFTI) file format. It also have 7 IVDs and lower spine from T11 to L5.
h) Dataset 8: It has four CT scans of lumbar spine having vertebral fractures. This dataset is actually the preview of CSI 2016 challenge [46].
i) Dataset 9: It consists of osteoporotic vertebral fractures, normal and non fractures cases' lateral and posterior-anterior PA scans acquired through dual energy x-ray absorptiometry (DXA) to detect the vertebral fracture.
j) Dataset 10: It consists of CT and MRI scan of 20 anonymous persons in axial and sagittal planes to understand the different poses and location of vertebra. [47]
k) Dataset 11: It contains various MRIs datasets from different hospital collected in time period of 5 years form 2009 to 2014. [48]
l) Dataset 12: It is the testing data of MICCAI 2016 challenge having 30 lateral and (PA) scans. It has three classes named as normal, other and compressed fractures and contains 10 scan each.
m) Dataset 13: It contains training and testing data of XVertSeg challenge. 15 CT scans were used as training data while other 10 were used as testing data.
n) Dataset 14: It has 24 different datasets of 3D multi modality MRI images collected from 12 patient after prolonged bed rest. This dataset was designed for MICCAI 2018 IVDM3Seg challenge.
o) Dataset 15: It contains test data of CSI 2014 challenges and consists of 10 CT scan of youngsters in between the age of 25 to 35 years [49].
p) Dataset 16: It consists of 609 spinal anterior posterior (AP) x ray scans and two expert doctors provided the corners offsets of this dataset in order to find the Cobb angles [50].

2. VerSe 2019: This dataset was designed for the VerSe 2019 challenge to gather researchers from all over the world to find the best algorithms for spinal labelling and segmentation. It contains 160 CT scans of 141 subjects [51].
3. VerSe 2020: It contains 300 Multi detector CT scans prepared for VerSe 2020 [52].

4. MyoSegmenTUM_spine: It contains 54 MRI images of 54 subjects [53]. This dataset is freely available for research.
5. Lumbar Spine MRI Dataset: This dataset has been posted on Mendaeley Data and contains MRI scans of 515 subjects with both axial and sagittal views. The sagittal view contains last 7 vertebrae 5 lumbar, 1 sacrum and a coccyx while axial view contains last three IVDs [54].
6. Lumbar Spine MRI Composite Dataset (CD): This dataset was originally taken from [54], which has axial views but they modified the dataset into sagittal views for effectiveness of results [55]. It also includes spinal measurements and pseudo colored ground truth images that contains 6 regions including 5 lumbar vertebrae and a sacrum.

The summary of all the datasets mentioned above is given in table 4.

Table 4: Different datasets used in researches

Datasets	**CT**	**MRI**	**X-Ray**	No of Images
Dataset 1	✓	✓		60
Dataset 2	✓			-
Dataset 3	✓			-
Dataset 4	✓			242
Dataset 5	✓			-
Dataset 6		✓		10
Dataset 7		✓		8
Dataset 8	✓			15
Dataset 9			✓	4
Dataset 10	✓	✓		-
Dataset 11		✓		-
Dataset 12			✓	-
Dataset 13	✓	✓		30
Dataset 14		✓		25
Dataset 15	✓	✓		10
Dataset 16			✓	609
VerSe 2019	✓	✓		160
VerSe 202	✓	✓		300
MyoSegmenTUM_spine		✓		54
Lumbar Spine MRI		✓		515
Lumbar Spine MRI Composite Dataset		✓		514

3.5 Gap Analysis & Contributions

The researchers have utilized different image processing and machine learning techniques for analysis of spine to identify different lumber deformities. Recently, utilization of deep learning has also been done for this purpose. However these methods face challenges in the presence of low contracts and noisy scans where vertebrae are not properly visible. The automated analysis of lumbar deformities relies on accurate localization of vertebrae and

even small variation in the centers can lead to false grading of deformities. Keeping all these gaps and challenges in mind, the contributions made in this research work are as following:

- This paper presents the object detection framework for lumbar deformities and provides the research community an annotated dataset in sagittal plane with labels in YOLO format.
- One of the major contributions of this research work is to utilize object detection/localization module as vertebrae localization in comparison to current state of the art methods which are based on semantic segmentation.
- A comparative analysis of different semantic segmentation models with proposed localization module has been performed to localize the lumbar and scrum vertebrae.
- Furthermore, we provide automated methods to calculate the angles to diagnose lumbar deformity such as lumbar lordosis and its further grading, which will be used as a decision support system for young radiologists and helps them to grade the severity of lumbar deformities.

CHAPTER 4: METHODOLOGY

This research has been done on [55] that contains sagittal views of MRI Images of 514 subjects. Our proposed approach is divided into two different techniques, in the first technique lumbar lordosis is assessed through localization while in second part localized vertebrae is passed through HED U-Net to get the segmented image and its edges. First we will discuss the localization of lumber and sacrum vertebrae followed by the overall proposed methodology.

4.1 Localization and Identification

Localization identify the location of the objects in an image and draws a bounding box around the objects [56]. Block diagram of first method is shown in Figure 4.1. Presented technique consist of preprocessing steps, training of YOLOv5 model, vertebrae localization, centroids calculations, area computation through centroids.

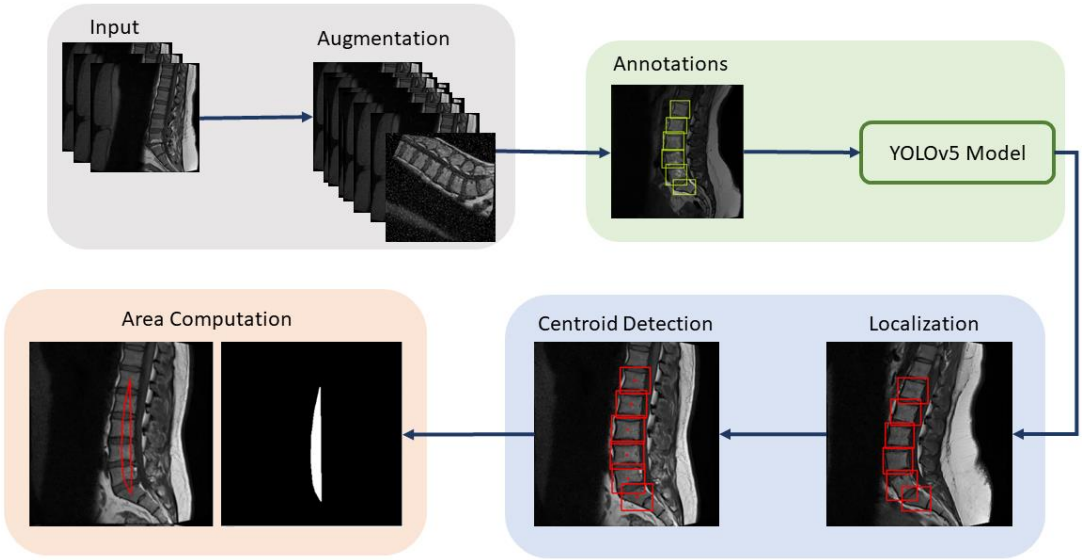

Figure 4.1: Localization and Identification Block Diagram.

4.1.1 Preprocessing

Preprocessing is the main and first step before training the model. Images are auto oriented and resized to 416x416. Other Preprocessing steps involved are data augmentation, data labelling and annotations.

4.1.1.1 Data Augmentation

Augmentation of dataset is necessary for better results, so the steps involved in augmentation are noise addition, image flipping, 90˚ rotation, image cropping, and image shearing. Salt and pepper noise is added to 5% of image pixels. Images are flipped to horizontal, 90˚ rotated to clockwise, counter clockwise and upside down, cropped to 0˚ minimum zoom and 20˚ maximum zoom, rotated between - 23˚ and +23˚ and sheared to ±15 horizontally and vertically.

Number of images are increased from 514 to 1028 after augmentation. Each image after augmentation has different values of each step. Figure 4.2 shows the augmentation of images, where (a) is -21˚ and 90˚ rotated, -6˚ and 13˚ sheared in X and Y direction and has 3% salt and pepper noise, (b) is -3˚ and 90˚ rotated, 4˚ and -3˚ sheared in X and Y directions with 0.25% noise, (c) is -4˚ and 90˚ rotated, -15˚ sheared in X direction and -4˚ is sheared in Y direction and has 0.25% noise.

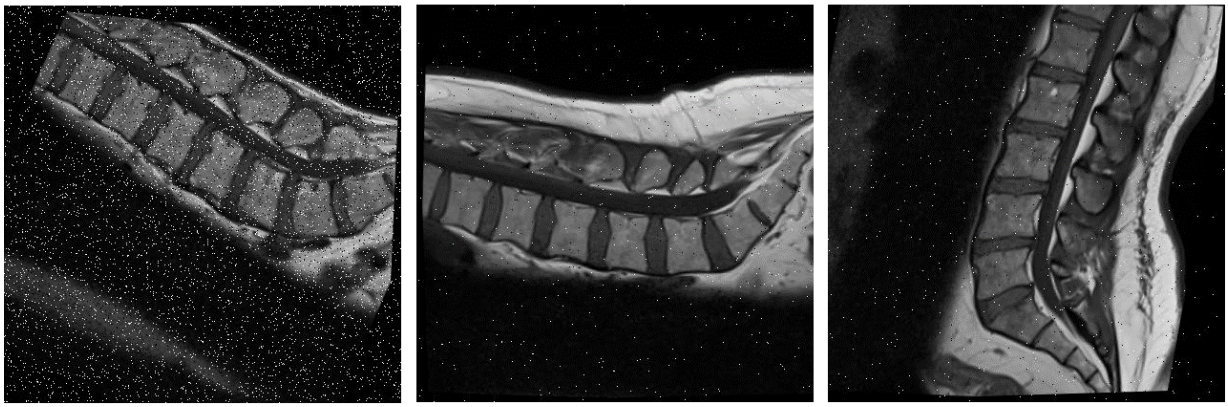

Figure 4.2: Augmented Images

4.1.2 Data Labelling & Annotations

We have used LabelMe and roboflow to label the dataset. Each image contains 6 annotations of a single class in YOLO format. YOLO format is txt file with same name as image that consists of class, x and y coordinates of object and width and height of object. Class name is defined as V for vertebrae and 6 labels contain 5 lumbar vertebrae and sacrum in sagittal view as shown in figure 4.3. Images are labelled in mid-sagittal view. Each image has the label file of the same name which is generated after labeling the image and it contains the class, centre coordinates and height and width of the objects that are lumbar vertebrae and sacrum bone in this case. We can calculate the coordinates of the bounding box by multiplying the coordinates, height and width of the objects with the height and width of the images which is 416 in this case.

$$x_{min} = (cen_x * width_{img}) - \frac{width_{obj} * width_{img}}{2} \quad (3.1)$$

$$y_{min} = \left(cen_y * height_{img}\right) - \frac{height_{obj} * height_{img}}{2} \quad (3.2)$$

$$x_{max} = (cen_x * width_{img} - \frac{width_{obj} * width_{img}}{2}) + (width_{obj} * width_{img}) \quad (3.3)$$

$$y_{max} = (cen_y * height_{img} - \frac{height_{obj} * height_{img}}{2}) + (height_{obj} * height_{img}) \quad (3.4)$$

In the above equations, $width_{img}$, $height_{img}$ are the width and height of image, $width_{obj}$, $height_{obj}$ are the width and height of object, cen_x and cen_y are the centre coordinates of object, and x_{max},y_{max}, x_{min}, y_{min} are the maximum and minimum coordinates of the bounding boxes.

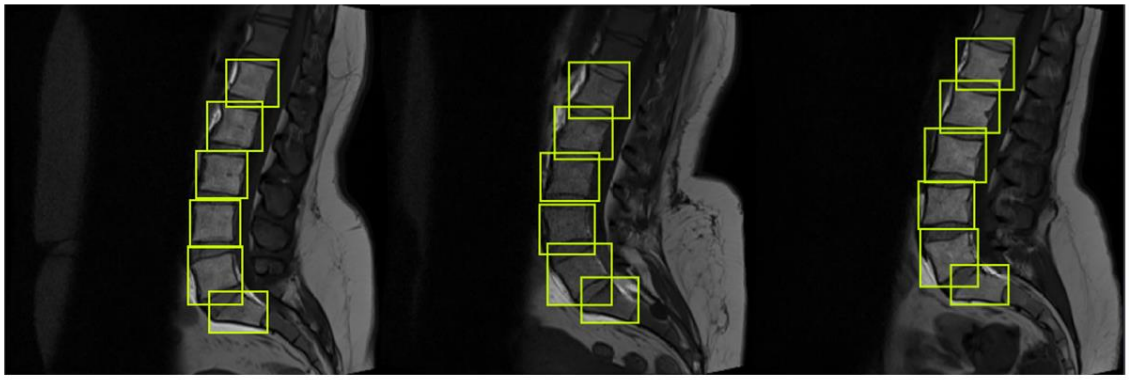

Figure 4.3: Labelled Images

4.1.3 Training

The annotated dataset is trained on YOLOv5 with 32 batch size and 90 epochs. Data is divided into 85% training, 10% validation and 5% testing. YOLOv5 has detected the lumbar vertebrae and sacrum with very good confidence score.

YOLO

YOLO stands for You Look Only Once and was developed in 2015 as an object detecting system using single neural network that contains multiple convolution networks. YOLO algorithm became very popular due to its high speed and accuracy. Object detection has been reframed as a single regression problem by YOLO, and this model predicts bounding boxes and class probabilities from image pixels. YOLO algorithm finds the bounding boxes of objects and probabilities of classes in boxes. Due to its good results in determining and detecting the object coordinates, it stands out than other object detection algorithms at the time of its release [57].

During the period of five years, YOLO algorithm has upgraded five different variants. The first three version of YOLO algorithms was developed by Joseph Redman. But after his discontinuation in computer vision research, the other two versions were developed by

different researchers. A Russian scientist published YOLOv4 and after one month YOLOv5 was released on the Pytorch framework by the researcher Glen Jocher with minor improvements and differences [57]. YOLOv5 outstands as compared to its previous versions in performance.

YOLOv5

YOLOv5 has 4 models, YOLOv5s, YOLOv5m, YOLOv5l, YOLOv5x. We have used the smallest and the fastest model YOLOv5s. It has a size of 14 Mb and has 2.2ms inference time. YOLOv5 consists of three stages: in the first stage data is fed into backbone which extracts the features, then it passes through neck in the second stage where the features are fused and third stage named as head outputs the detection results [58].

YOLOv5 network architecture is shown in figure 4.4. The three stages are as follows:

CSPNet: Backbone

YOLOv5 includes cross stage partial network (CSPNet) [59] into darknet and makes CSPDarknet its backbone. It decreases the model's floating point operations per second (FLOPS) and parameters by solving the problem of repeated gradient information in large scale and integrates the gradient changes into feature map. This not only reduce the size of model but also ensure the accuracy and speed of inference.

PANet [60]: Neck

It increases the flow of information through pipelining. Low level features can be propagated efficiently by adding Feature Pyramid Network (FPN) which is new feature with properties like bottom up path augmentation. Feature grid and all other features are linked together by adaptive pooling which makes the useful information in each feature level. Network decides which features are useful from all the layers. It increases the accuracy of object location by using the correct localization signals in lower layers [58].

YOLO Layer: Head

This is last layer of YOLOv5, which detects the results in form of confidence score, size, and accuracy. It contains three different types of feature maps i.e, 18x18, 36x36, 72x72 to detect small, medium and big objects [58].

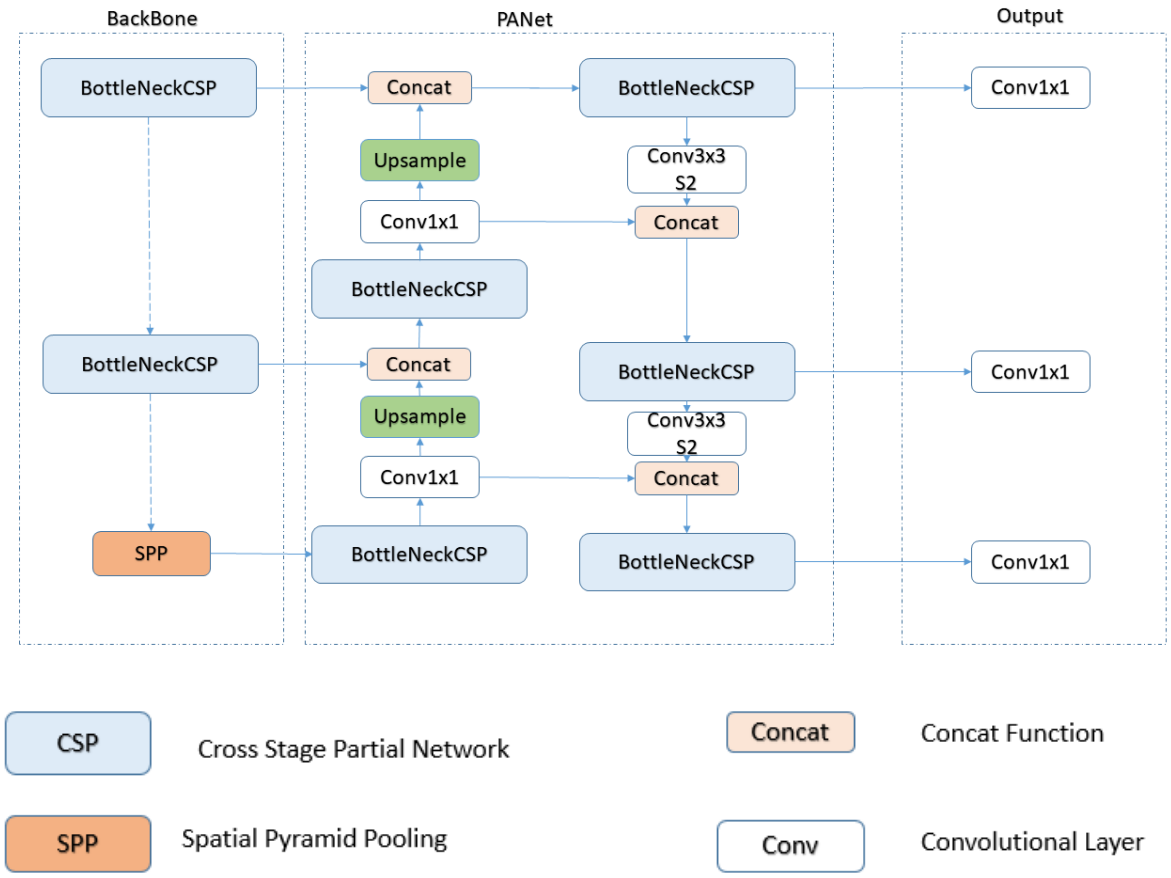

Figure 4.4: YOLOv5 Network Architecture

4.1.4 Vertebrae localization and Centroids Calculation

Vertebrae is localized with a very good confidence score as shown in the figure 4.5. An empirical threshold of 0.65 has been applied on confidence score to eliminate the boxes with less score. The IOU threshold is set to 0.3 in testing data.

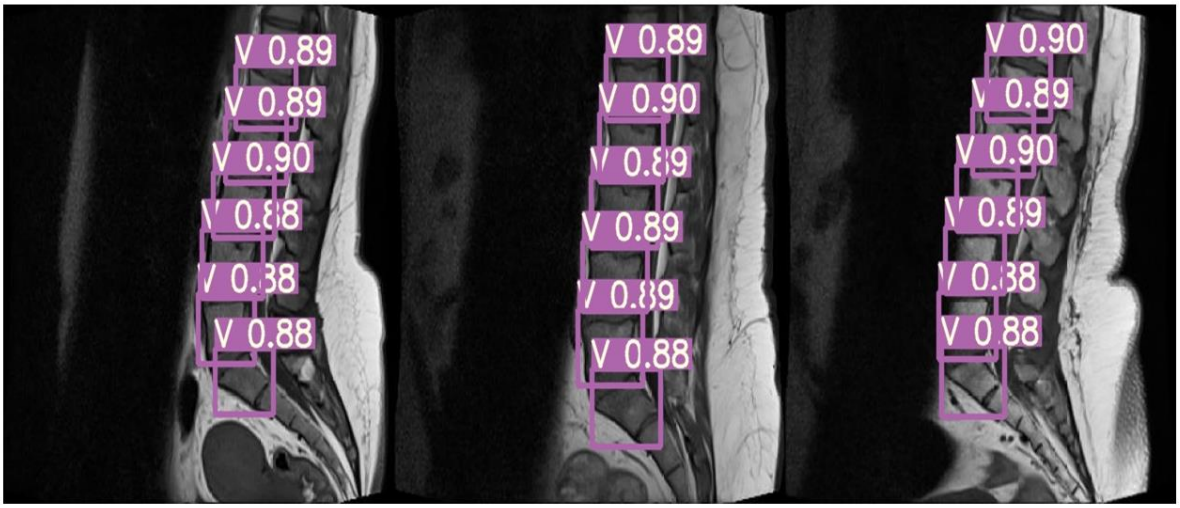

Figure 4.5: Predicted YOLOv5 Images with Confidence Scores

Bounding boxes are drawn across each vertebra to find the centroids of boxes. The ground truth and predicted centroids are measured by following formula:

$$Centre_{x,y} = \frac{x_{min}, y_{min} + x_{max}, y_{max}}{2} \tag{4.1}$$

Where x_{min}, x_{max}, y_{min} and y_{max} represent the x and y coordinates of bounding boxes. The ground truth and predicted centroids are shown in green and red colors in figure 4.6. In Figure 4.6(a) green bounding boxes represents the ground truth boxes with their centroids while in figure 4.6(b) red bounding boxes represents the predicted bounding boxes with their centroids.

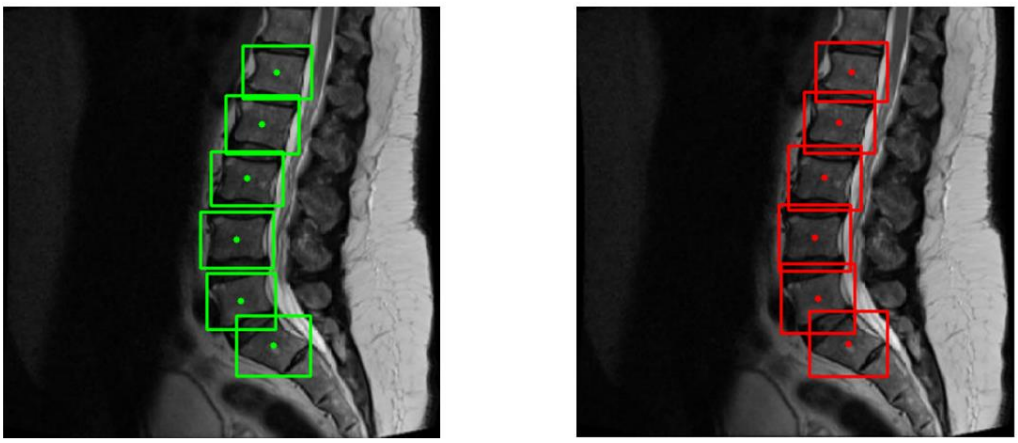

(a) (b)

Figure 4.6: Ground Truth and Predicted bounding boxes

4.1.5 Area Region Calculation

[37] have proposed the method to diagnose lordosis on the basis of area enclosed in the region. They have combined [61] and [62] techniques to get the area under the curve from the centroids. We have computed the area from the centroids of the bounding boxes of YOLOv5 as shown in figure 4.7. Centroid of L1 is connected to L2, L2 to L3 and so on, and lastly centroid of S is connected to L1, to form enclosed region. The normal range for lordosis is 39˚ to 53˚ [63]. Angles below 39˚ are termed as hypo lordosis while the angles above 53˚are termed as hyper lordosis. Area of enclosed region is correlated with the angles to diagnose the disease. Area can be found by summing all the non-zero pixels in the images. The equation is given by:

$$Area_{region} = \sum_{i=0}^{total_n} zz_i \times \Delta zz \tag{4.2}$$

$Area_{region}$ represents the area of the region, zz_i is the non-zero pixels in the images, Δzz is the interval between pixels and is equivalent to one pixel. This method was proposed by [37] to diagnose the lordosis from the centroids instead of corner points.

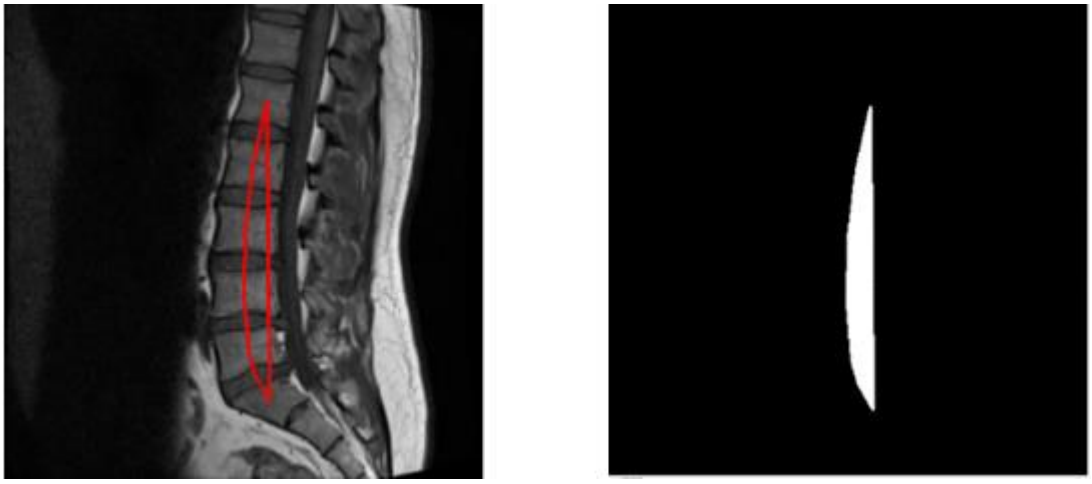

(a) (b)

Figure 4.7: Area Computation by counting the non zero pixels

4.2 Overall Proposed Methodology

Our proposed methodology consists of same few steps done by YOLOv5 in localization and identification part. The annotated dataset is passed through YOLOv5 to get the localize vertebrae. Bounding boxes across each vertebrae is used to crop the images. Binary masks were created to pass the localized vertebrae through HED U-Net to get the segmented images and their detected edges, extracted images are smoothed and corners are found and lastly lines are drawn to find the angles. The figure 4.8 shows the flow of our proposed methodology where dataset is localized and then passed through HED U-Net. L1 and S for LLA and L5 and S for LSA are extracted from the localized image. Images are smoothed using gaussian smoothing filter and Harris corner detector are applied to get the corners of desired vertebrae. LLA and LSA can be found from the corners.

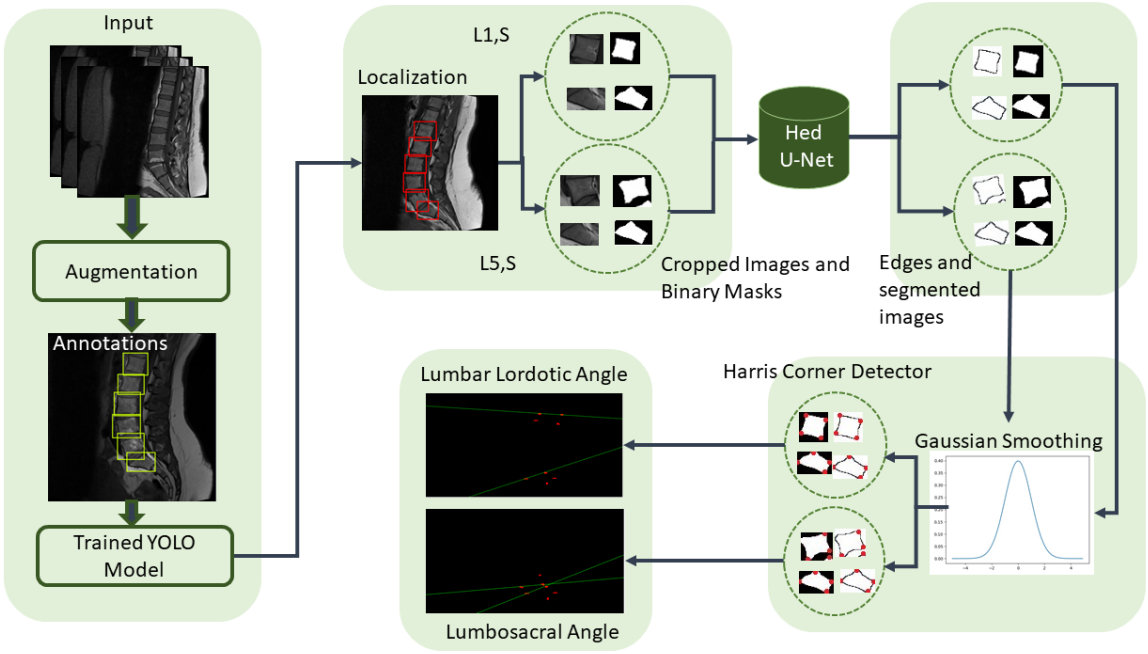

Figure 4.8: Proposed Framework

4.2.1 Localization

This part consists of same few steps we have done in localization and identification part. Images from the dataset are augmented, annotated and passed through YOLOv5 to get the localized lumbar spine and sacrum. Bounding box is drawn across each vertebra. We cropped L1, L5 and S through the bounding boxes and passed these images through the HED U-Net.

4.2.2 Training

Cropped images with their binary masks are passed through the HED U-Net. The batch size is set to 8 with epoch size 10, learning rate 0.001 and optimizer as Adam.

HED U-Net

Heidler in [64] developed HED U-Net which is a combination of segmentation and edge detection framework. They unified the U-Net [65] for semantic segmentation and HED [66] for Edge detection in a natural way. In our case of segmentation there are two class labels i.e, vertebra and background and in case of edge detection there are two classes which are “no edge” and “edge”. Figure 4.9 shows the high level representation of the HED U-Net, image is passed through the encoder where down sampling of image is performed to accumulate the contextual information at low resolution. Then decoder upsamples the image by distributing this information to individual pixels. In this model, the researchers used 6 resolution levels of feature pyramid, where the full image resolution has the finest feature map and poor feature

map at resolution 1/32 [64]. The model is deep supervised where it is trained to predict the ground truth at every level of feature pyramid. Deep supervision is used to increase the generalization capacity and learning efficacy of a model. Then there is two task specified merging head which uses hierarchy attention mechanism to combine this information. In this mechanism most useful features of each pixel are focused rather than fused features of fix weights [64].

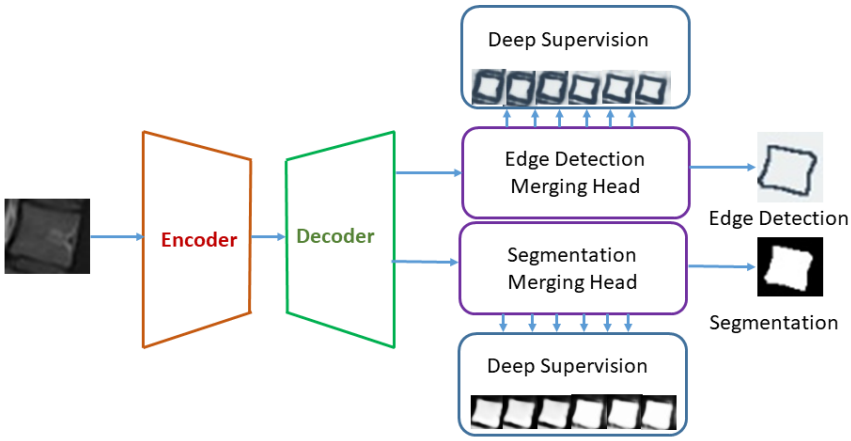

Figure 4.9: High Level Structure of HED U-Net

4.2.3 Image smoothing and Corner calculation

After the images are passed through HED U-Net, we get the segmented image and the detected edges. We have cropped the images from the bounding boxes we got from YOLOv5. We have to compute the LLA and LSA. LLA is the angle between the L1 superior endplate and S superior endplate while LSA is the angle between the L5 inferior endplate and S superior endplate, so we used the bounding boxes of L1 and S for LLA and L5 and S for LSA to crop the desire vertebra. To get the smooth image the vertebra images are then passed through the Gaussian Smoothing Filter with the sigma value equal to 1 which helps us in finding the corners through Harris corner detector [67] accurately. Harris corner Detector is applied on the smoothed images to get the corners of L1 and S for LLA and corners of L5 and S for LSA. Figure 4.12 and figure 4.13 show the extracted L1 and S with their corners for LLA and extracted L5 and S with their corners for LSA.

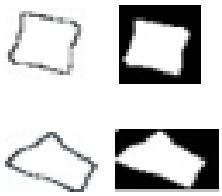

Figure 4.10: Segmented Images of L1 and S with their detected edges

Figure 4.11: Segmented Images of L5 and S with their detected edges

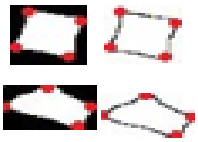

Figure 4.12: Smoothed L1 and S corners through Harris corner detector

Figure 4.13: Smoothed L5 and S corners through Harris corner detector

4.2.4 Angles Computation

In case of LLA, a line is drawn from the superior corners of L1 and other line is drawn from the superior corners of S, while for LSA one line is drawn from the inferior corners of L5 while other is drawn from the superior corners of S. The slope of the lines can be found from the following formula:

$$m_{L1,S} = \frac{p2_y - p1_y}{p2_x - p1_x} \tag{4.3}$$

m represents the slope of lines, $p1_y$ and $p2_y$ are y axis points while $p1_x$ and $p2_x$ are the x axis of two points. The angle between the lines can be found from the below expression:

$$Angle = tan^{-1}\left|\frac{m_{L1} - m_S}{1 + m_{L1}m_S}\right| \quad (4.4)$$

m_{L1} is the slope of superior endplate of L1 line while m_s is the slope of superior endplate of S line. The same equations can be used to find the slope and angle for LSA.

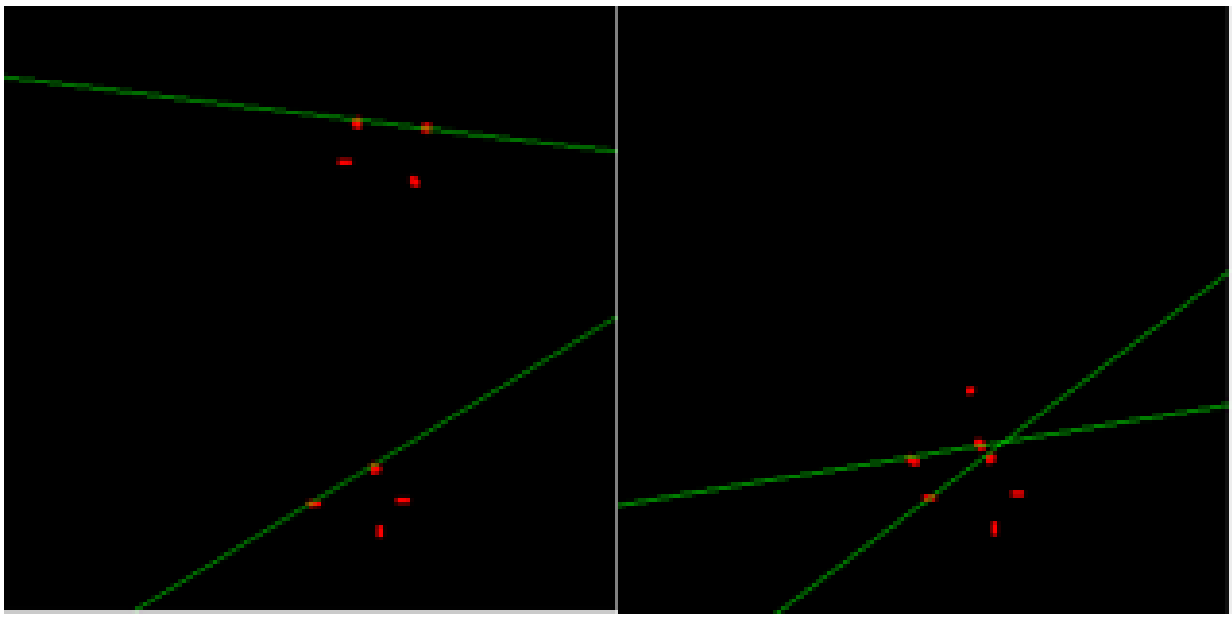

Figure 4.14: Slope and angle can be find from lines.

We have used two methods for the lumbar lordosis assessment. The first part only consist of localization part and second part consists of both the localization and edge based segmentation. In first method, lordosis is assessed through the region area which is computed through centroids of vertebrae and the value of area is correlated with the ground truth values while in our overall proposed methodology the lordosis is assessed through the angle value which is calculated from the corners of the vertebrae. Our proposed method consists of two parts, the first part is the localization and the second part is edge based segmentation. After the vertebra is passed through the Harris corner detector, intersecting angles can be found from the corners of the vertebra.

CHAPTER 5: EXPERIMENTAL RESULTS

5.1 Databases

To diagnose the spinal deformities, number of datasets have been developed by hospitals and challenges. Evaluation of our proposed methodology is performed on Lumbar Spine Composite dataset.

5.1.1 Lumbar Spine Composite Dataset

Lumbar Spine Composite Dataset [55] has been posted on Mendeley Data and was originally taken from MRI Dataset [54]. Original dataset has annotations of axial views while [37] has annotated the dataset into mid-sagittal views for effectiveness of results. It also includes spinal measurements, ground truth labels and pseudo colored ground truth images. Spinal measurements help surgeons in suggesting and selecting the appropriate surgical procedure. MRI dataset has data of 515 subjects, while [54] discarded one subject due to noisy picture and has data of 514 subjects, with ground truth and pseudo colored labels available for the segmentation. The resolution of the images and labels are 320x320. Figure 5.1 shows images from composite dataset. Figure 5.1(a) and 5.1(b) represent the mid-sagittal view of Lumbar spine with their respective pseudo colored labels.

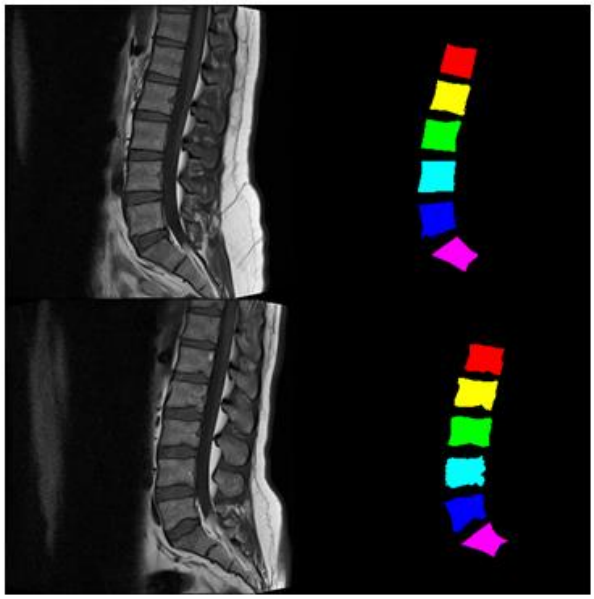

(a) (b)

Figure 5.1: Images with their respective pseudo label

Following steps has been applied on MRI dataset to acquire composite data:

- Dicom viewer is used to read the image and mid-sagittal view has been exported from MRI dataset.
- Images are manually labelled from lumbar spine to first sacrum vertebra after obtaining the sagittal view.
- Labelled regions are consulted with radiologists and validated by expert surgeons.
- Labelled are assigned and pseudo coloring has been applied where each vertebra is represented by different color.
- Fully automated spinal measurements have been performed that contains Lumbar Lordotic Angle (LLA), Lumbosacral Angle(LSA), dimensions of lumbar spine and sacrum and their identification and labelling, height of lumbar spine, dimensions of discs, spinal curve estimation.

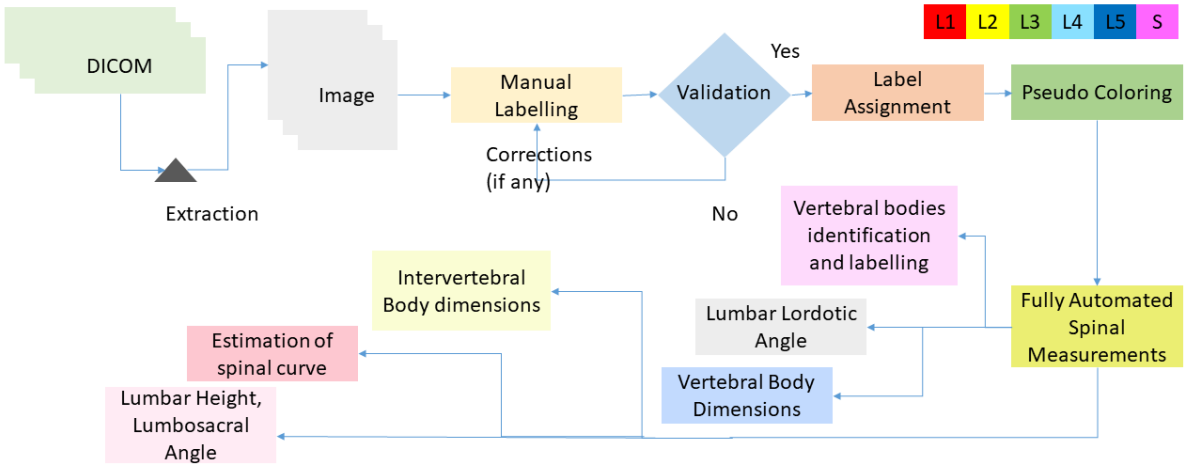

Figure 5.2: Flow diagram of lumbar spine composite dataset.

5.2 Evaluation Measures

To measure the performance of our methodology for localization, we have used Euclidean Distance (EU) and intersection over union (IOU) metrics. Distance between the centroids is calculated by EU. The equation for the EU is given below:

$$EU = \sqrt{(x_2 - x_1)^2 + (y_2 - y_1)^2} \quad (5.1)$$

x_1 and y_1 are the centroids coordinates of ground truth boxes while x_2, y_2 are the x and y axis of predicted boxes. Each image contains seven EU, one for each class. Less value of EU

indicates less error of distance between the centroids of predicted bounding box with ground truth box. All the measurements taken on the image are in mm. Overlap of ground truth box and predicted box is measured through IOU. To find the IOU, following formula is used:

$$IOU = \frac{Area.of.overlap}{Area.of.union} \tag{5.2}$$

IOU is the ratio between area of two boxes overlap and the total area of two boxes as shown in equation 5.2. More the value of IOU, more is the overlap of two boxes. If the value of IOU comes 0.95, it means the two boxes are overlapped by 95 percent.

To evaluate the segmentation part, we have used IOU and Dice Coefficient score (DC). IOU can be found from the equation 5.2, while DC can be found from the following formula:

$$DC = \frac{2 * Area.of.overlap}{Total.number.of.pixels} \tag{5.3}$$

DC can be defined as the ratio between the overlapped **areas** times two and the total number of pixels in the images. Its value is between 0 and 1, value near to 1 depicts good DC of model.

$$ME = \frac{1}{k}\sum_{l=0}^{k-1}\left|a_{pred} - a_{orig}\right| \tag{5.4}$$

ME represents the mean absolute error of angles and its value is in degrees, that calculates the error in the estimated and predicted angles. Lesser value of ME shows less error between the predicted and ground truth values. k is the total number of images, a_{pred} is the an angle predicted while a_{orig} is the ground truth value of an angle.

5.3 Results & Discussion

We have accessed lumbar lordosis through two ways, all the results are discussed in this section. The comparison of different segmentation models are also present in this section. The proposed approaches have been trained on RTX 2070 GPU with 16GB ram and implemented in Python using Pycharm and Anaconda.

We have used [55] that contains 514 images. After augmentation in localization part, data has been increased to 1086 images. Various deep learning techniques have applied on the same dataset, but we have used object detector for the localization of lumbar spine and sacrum and labelMe python package for data annotations and saved it in YOLO format. After training and testing the model, the ground truth and predicted bounding boxes are compared by EU of centre points.

Mean of EU between the centroids of bounding boxes and IOU of two boxes can be calculated from the following formula:

$$M_{EU} = \frac{\sum_{l=0}^{F-1} EU_l}{F} \tag{5.4}$$

To calculate the mean of IOU of each vertebra, following equation is used:

$$M_{IOU} = \frac{\sum_{l=o}^{F-1} IOU_l}{F} \tag{5.5}$$

In the above equations, F represents the total number of image, EU_l is the centroid distance, IOU_l is the intersection over Union, M_{EU} and M_{IOU} represent the mean of EU and IOU of each vertebra.

Standard deviation measures the deviation of value from mean value and can be measured from following formula:

$$St.D_{EU} = \sqrt{\frac{\sum_{l=0}^{F-1}(EU_l - M_{EU})^2}{F}} \tag{5.6}$$

$$St.D_{IOU} = \sqrt{\frac{\sum_{l=0}^{F-1}(EU_l - M_{IOU})^2}{F}} \tag{5.7}$$

where $St.D_{EU}$, $St.D_{IOU}$, F, EU_i, IOU_i, M_{EU}, M_{IOU} show the standard deviation of EU and IOU, total no of images, EU of centroids, IOU of boxes, mean of EU and IOU.

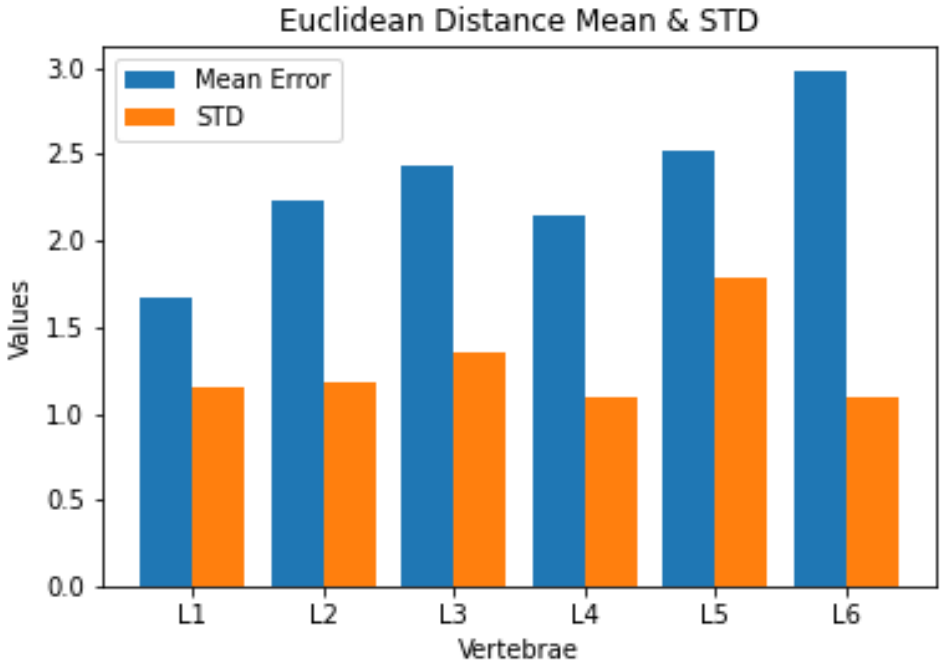

Figure 5.3: Mean and St.D of EU

Figure 5.3 shows the mean and standard deviation of EU. Blue bar represents the mean while orange bar represents the STD of mean. L1 has lowest value of mean and L6 has the highest value of mean among all the vertebrae. It shows the mean and the standard deviation of 6 vertebrae separately. The distance between the centroids are in millimeters, sacrum has the highest EU mean due to its tilted structure, while L1 has the least EU mean of 1.6 mm. Low value of mean indicates less distance between the centroids. Figure 5.4 shows the mean and standard deviation of IOU of each vertebra. Each vertebrae has high value of mean and low value of standard deviation. High value of mean shows higher overlap between the bounding boxes. Blue bar represents the mean and orange bar represents the std of IOU mean. L1 has the highest value of IOU mean with lowest value of std.

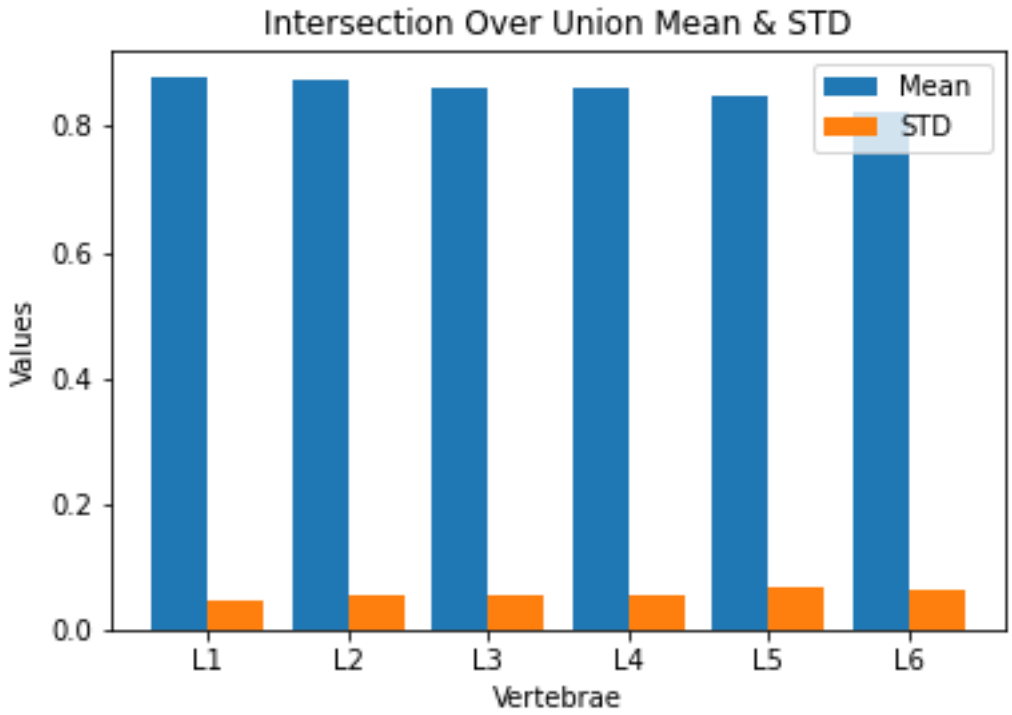

Figure 5.4: Mean and St.D of IOU

Average precision is use to evaluate the accuracy of YOLOv5, it calculates the average precision values for over a 0 or 1 recall value. Figure 5.5 shows the values of Precision and Recall of object detector YOLOv5 with increasing values of epoch from 0 to 90.

Precision It is defined as the ratio of true positive cases and total number of true predictions.

$$P = \frac{True.Positive.Cases}{Total.Positive.Predictions} \tag{5.8}$$

Recall It is defined as the ratio of true positive cases and the total number of cases.

$$R = \frac{True.Positive\ .Cases}{Total.Cases} \tag{5.9}$$

Mean Average Precision mAP is the mean of average Precision, we have got mAP of 0.975 by using YOLOv5s as shown in the figure 5.5. Figure 5.5(a) and (b) represent the Recall and Precision values of YOLOv5s during training with increasing epochs, (c) mAP@0.5 represents mAP values with the IOU threshold value as 0.5 (d) mAP@0.5:0.95 represents mAP values with different IOU threshold values that range from 0.5 to 0.95 with step size of 0.05.

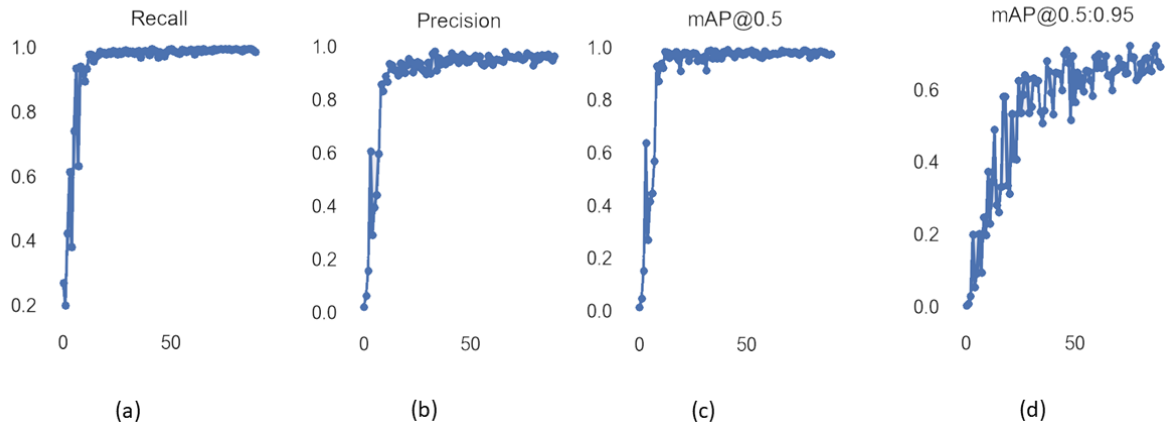

Figure 5.5: (a), (b), (c) and (d) represent the recall, precision, mAP of yolov5

Before applying non maximum suppression, YOLOv5 can be visualized in heatmaps from its original weights as shown in figure 5.6.

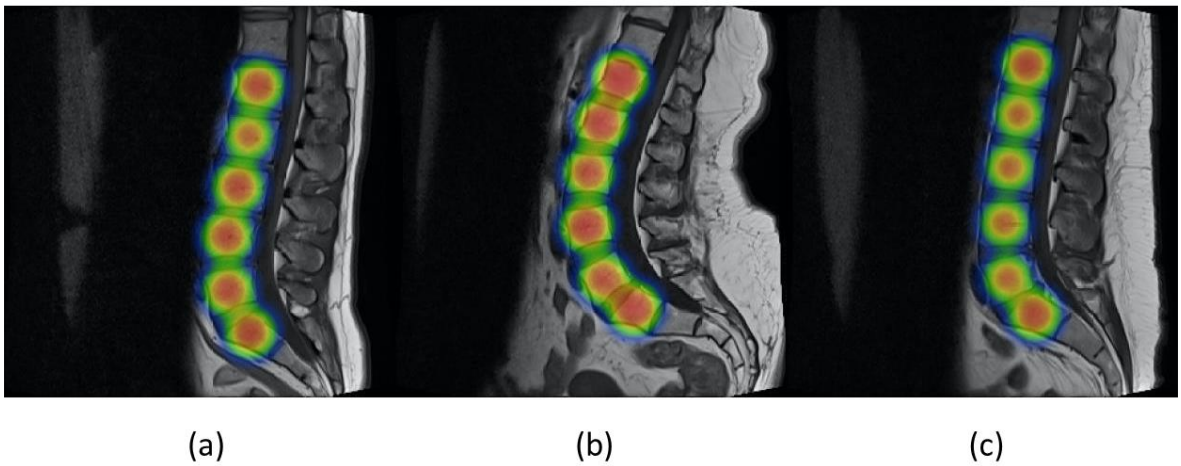

Figure 5.6: YOLOv5 visualization in heatmaps obtained from its weights after training.

Figure 5.7 shows three images each from different lordosis type. Each column represents the region plot of an image and its respective area computation image. Figure 5.7(a), (b) and (c) represent the hypo lordosis, normal lordosis and hyper lordosis cases respectively. Each image has different curve and area which differentiates the disease. Hypo lordosis includes straight back and flat back cases, while hyper lordosis includes sway back of the vertebrae. The region area of normal lordosis is less than the hyper lordosis and greater than the hypo lordosis curve [37]. We have got 74.5 percent accuracy by using this technique.

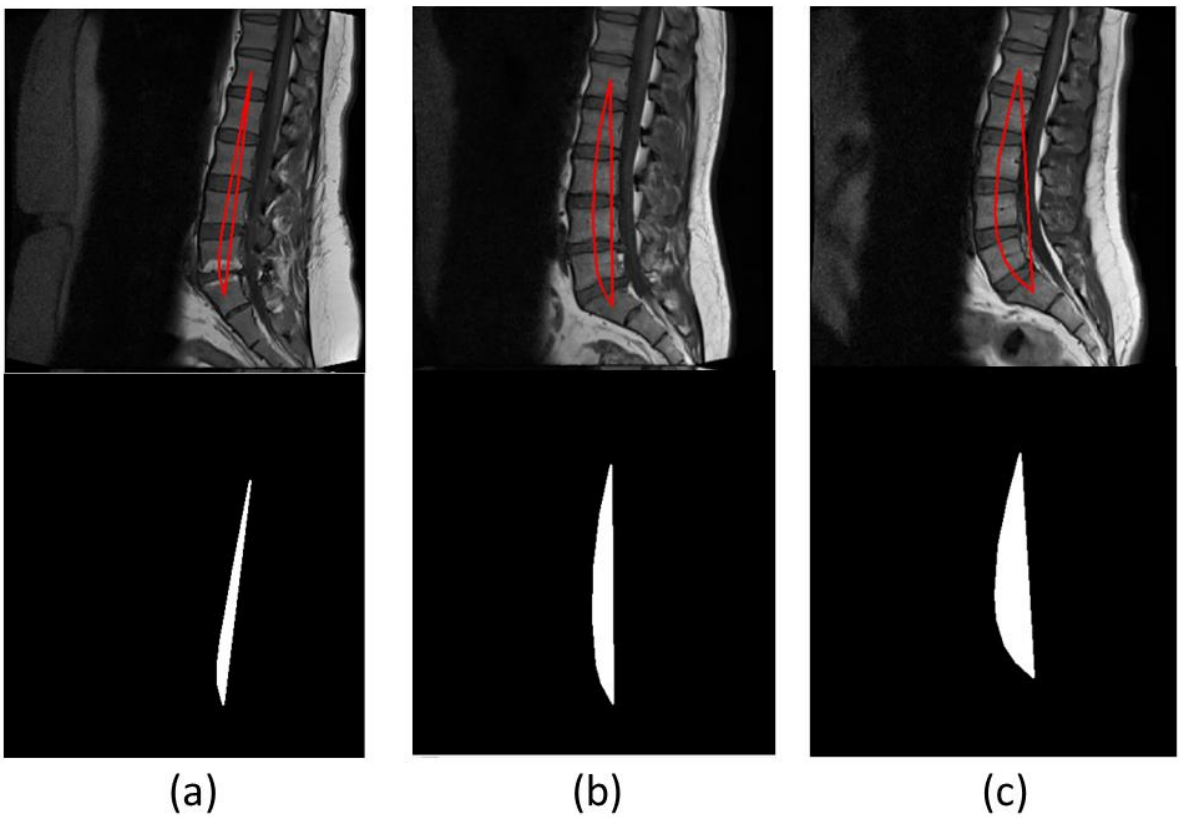

Figure 5.7: (a), (b) and (c) show the hypo, normal and hyper lordosis respectively.

Table 5 shows the confusion matrix for this technique, we have some of the failures cases in case of normal and hyper lordosis. Hypo lordosis has no failures cases while normal lordosis has 8 and hyper lordosis has 5 failures cases. 6 normal cases of normal lordosis lie in hypo while 2 cases lie in hypo lordosis. 5 failures cases of hypo lordosis lie in normal lordosis.

Table 5: Confusion matrix of Lumbar lordosis assessment through region area

	HYPO	**NORMAL**	**HYPER**
HYPO	6	0	0
NORMAL	6	11	2
HYPER	0	5	21

Figure 5.8 shows the boxplot values of calculated and ground truth angles of 3 classes calculated from the segmentation part. It shows that all the predicted and original angle values of each class lie in the same range. As mentioned earlier normal LLA ranges from 39˚to 53˚, so angles less than 39˚are in the range of hypo lordosis named as class 0, normal lordosis is class 1 and class2 is hyper lordosis having angle values above 53˚. The boxplot shows very less error between the calculated values and ground truth values of angles. According to [68] [69] [70], the measurement error up to ±3˚-±5˚ is clinically accepted.

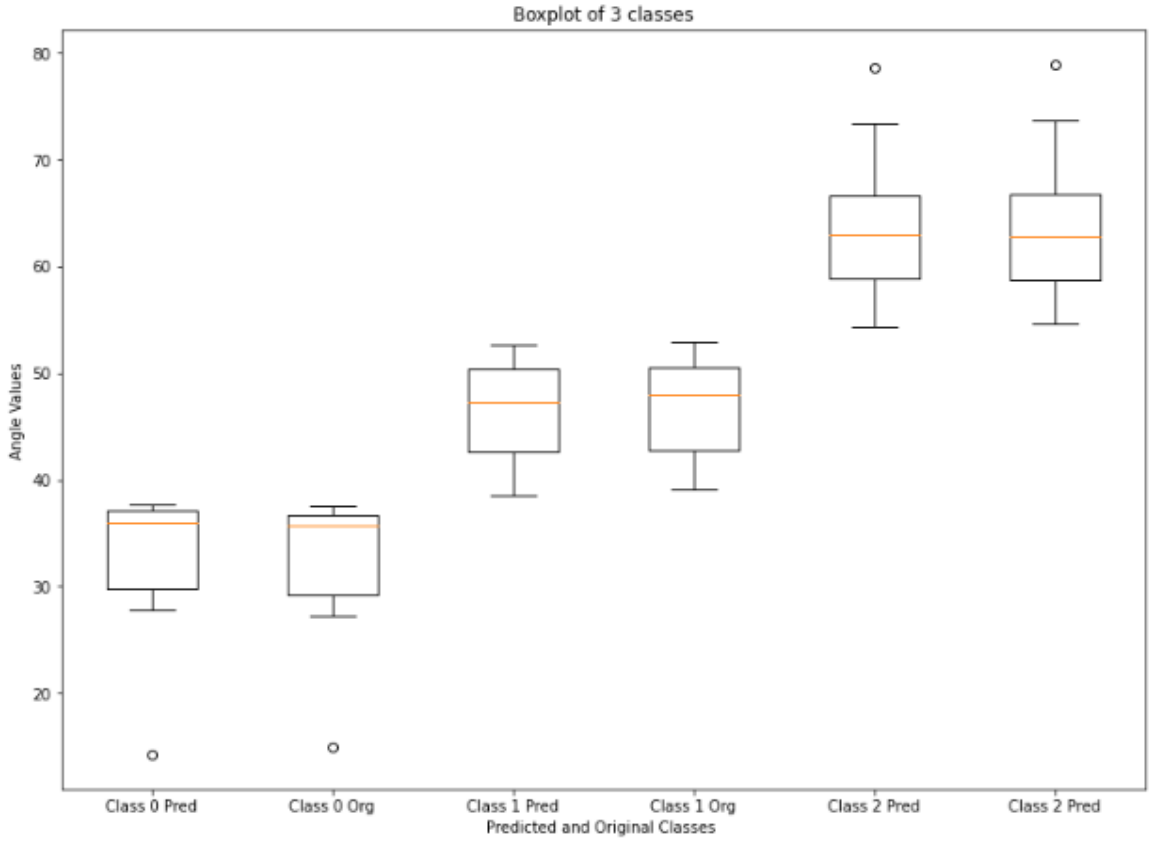

Figure 5.8: Boxplot of Hypo, Normal and Hyper Lumbar Lordosis

The mean error and standard deviation of mean error of LLA and LSA are shown in figure 5.9. Blue bar represents the mean error while orange bar represents std of mean error. LLA has low mean error and std than LSA mean error and its std. LLA and LSA calculated from our method have very less mean error values i.e., 0.29˚ and 0.38˚.

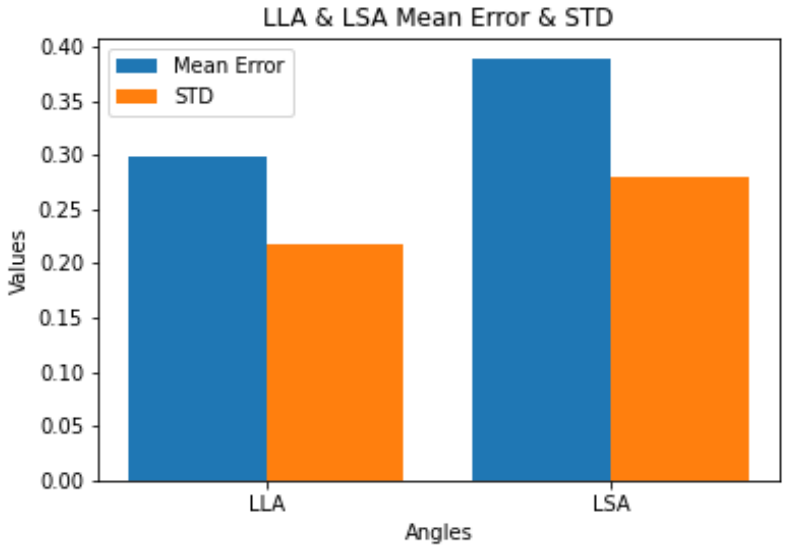

Figure 5.9: Mean error and ST.D of LLA & LSA

Confusion matrix for this technique is shown in table 6. There is no failure cases in any of predicted classes due to less error between ground truth and predicted angles values.

Table 6: Confusion matrix of Lumbar Lordosis Assessment through corners of vertebra.

	HYPO	**NORMAL**	**HYPER**
HYPO	6	0	0
NORMAL	0	19	0
HYPER	0	0	26

5.3.1 Comparison of Different Segmentation Models

Different deep learning models has been applied on the dataset to get the desired segmentation results. Deep learning models are evaluated on the basis of DC and IOU. We have used [55] annotations for segmentation. Data is passed through three models U-Net, SegNet and Fcn_32.

U-Net

Olaf Ranneberger et al. in their research paper have proposed new framework U-Net for bio-medical image segmentation. U-Net architecture is size invariant network that accepts images of any size [64]. As the name suggest this network shaped as U as shown in figure 5.10 which perform with total 23 convolutional layers. The left side is contracting path and the right one is expansive path. The input image is passed to a block which contains 2 convolutional layer with kernel size of 3x3 which is unpadded with relu activation, escorted with max-pooling. Due to 2x2 max pooling with stride 2 reduces size of feature maps, doubling the number of feature channels at each down sampling step. Four iterations of concatenation involve expansion paths that are branched for the up-sampling of the reduced feature maps. The termination layer of 1x1 convolution to get desired number of classes. This framework does not have any fully connected layers. It allows seamless segmentation with overlap-tile strategy.

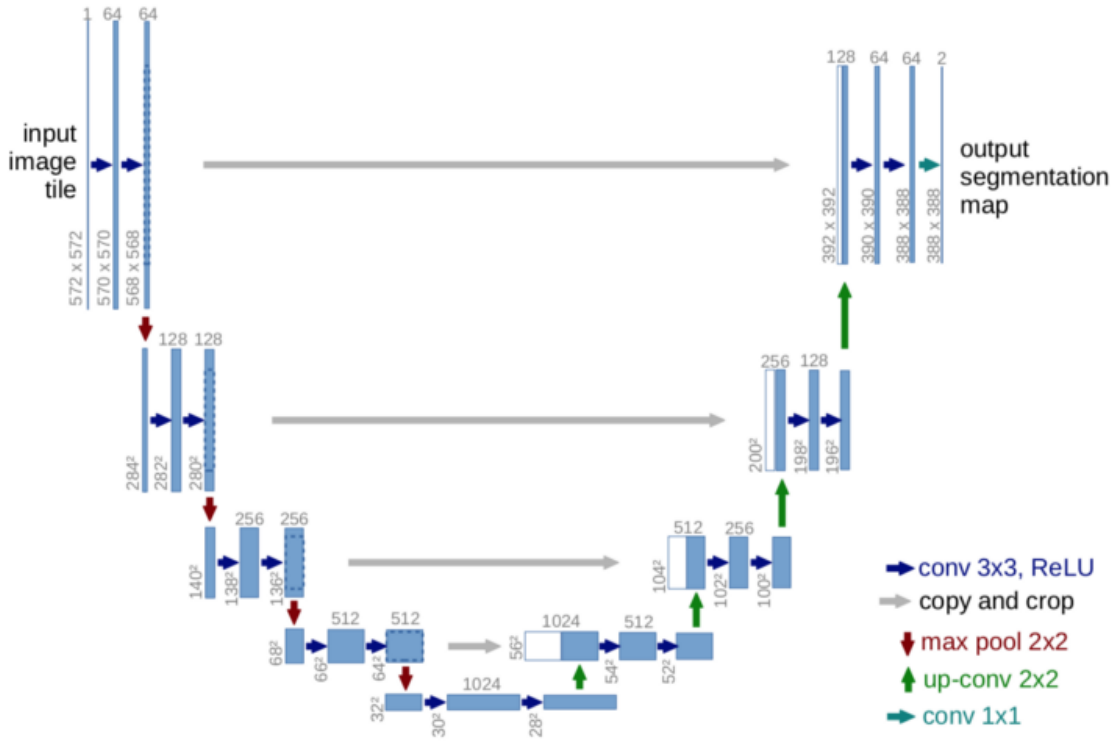

Figure 5.10: U-Net Architecture

Figure 5.10 represents every blue bar contacts with multi-channel feature map. On the top of each bar total no of channels shown and the size x and y is given at the edge of the bar. Empty white bars indicate copied features.

SegNet

SegNet is basically designed for the semantic segmentation of an image. [71] have proposed a deep learning model that comprises of encoder and decoder architecture, encoder architecture is similar to 13 VGG16 convolutional layers network, it saves the contextual information and stores the pooling indices while doing max pooling of 2x2 with non overlapping window and a stride of 2 that will sub-samples the image by 2. Decoder non-linearly up-samples the feature map by using the pooling indices that was computed in encoder section. Up-sampling is done to preserve the size of an image due to which the output image has the same size as input. It has less trainable parameters which makes it efficient in computations. The final decoder is attracted to the softmax classifier that classifies each pixel.

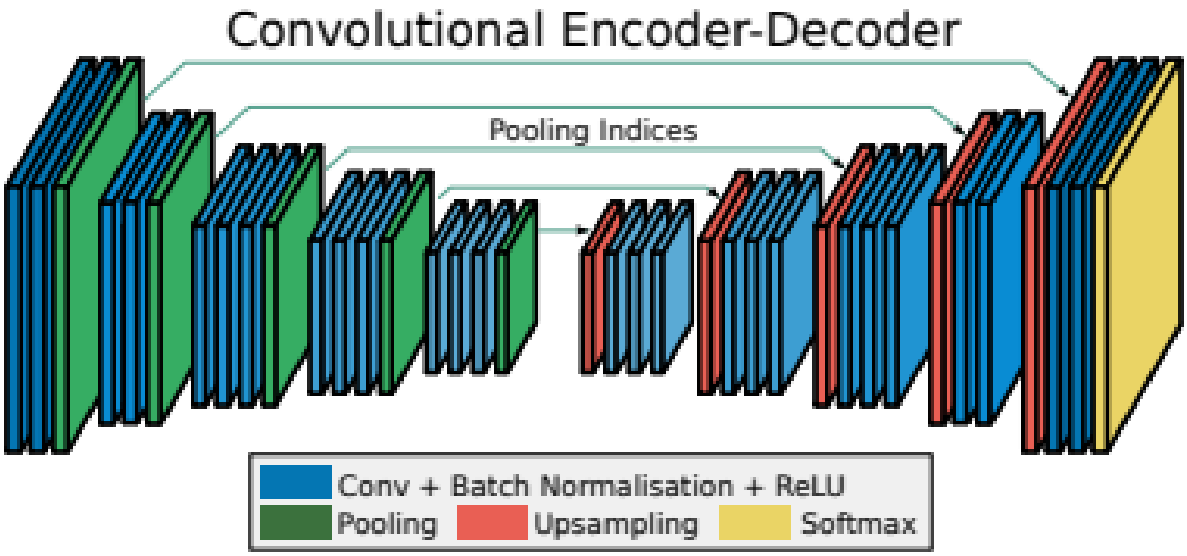

Figure 5.11: SegNet Archietecture [71]

FCN

Fully convolutional networks for semantic segmentation were proposed by Jonathan Long et al. in 2015. FCN is kind of networks that harvest hierarchies of features. As we know CNN itself works with pixel-to-pixel semantic segmentation on any dimensional input image. While connected layer require input image of fixed size so FCN comes here to connect CNN with connected layers where each node is connected to following layer. With the help of FCN, you can have input image of any size and get corresponding predictions. FCN does dense prediction and works effectively by combination of convolution and pooling layers to learn features in an image. One can say that the basic idea behind FCN is to take input image to produce output of very same dimension with no. of classes as the channel. FCN has 6 convolutional stages of any size in first stage dimension remains the same but in sixth stage the input size reduces to 1x32 leading for dense prediction layer with up sampling. The key factor of FCN is that it is size invariant but computationally expensive as number of floating-point operations are required to process [72]. FCN has many different architectures as shown in figure 5.10 and all of them give different outputs. All have the same downsampling path but different upsampling path, and they all differ in skip connections and last convolutional layers [73]. We will be using FCN_32 in our proposed technique.

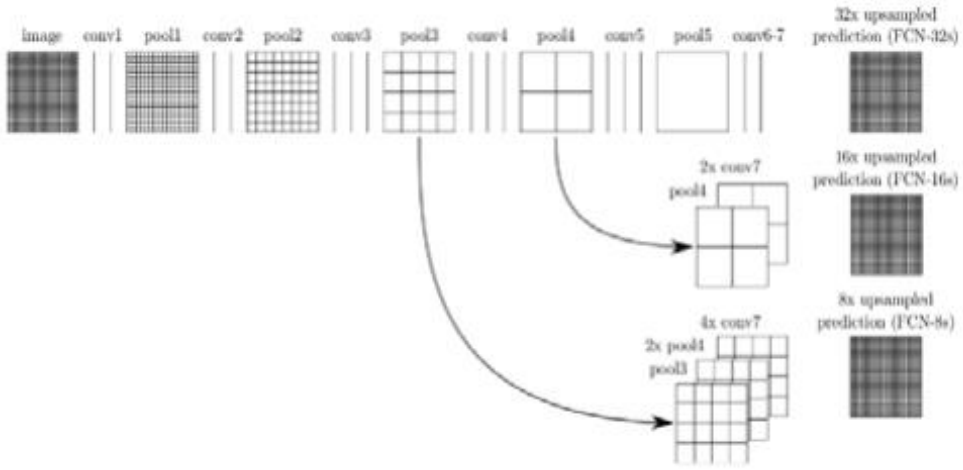

Figure 5.12: Different FCN models [73]

Segmentation results are shown in figure 5.13. Each color represents different vertebra. The segmented image has vertebra from L1 to L5 and a sacrum. Row represents the same model used for segmentation of various samples while the column represents different models used to segment the same sample. Row 1 represents the segmentation results of U-Net, Row 2 represents the segmentation results of SegNet and Row 3 represents the segmentation results of FCN_32. Each row has best and worst segmented cases. Each row has different samples of images using same segmentation model. Although models have less difference between them in terms of DC and IOU, but still it is clear that U-Net outperforms other models. In the qualitative results, it can be seen in the third and fourth column that SegNet results have a part of an extra vertebra. FCN_32 model has segmented all the vertebra but it shows less overlap as compared to U-Net and SegNet. DC and IOU are calculated by using the equation 5.2 and 5.3 and the results of all the three models are shown in the table 3. Bold values of Dice Coefficient and IOU show the model that outperforms other models. DC and IOU values range from 0 to 1, where the value closes to 0 means less overlap between the ground truth and segmented images while values close to 1 means good overlap between ground truth and segmented image and better performance of the model. Bold values of DC and IOU shows the highest value we got from U-Net model. SegNet and FCN_32 have slightly less DC and IOU from the U-Net model.

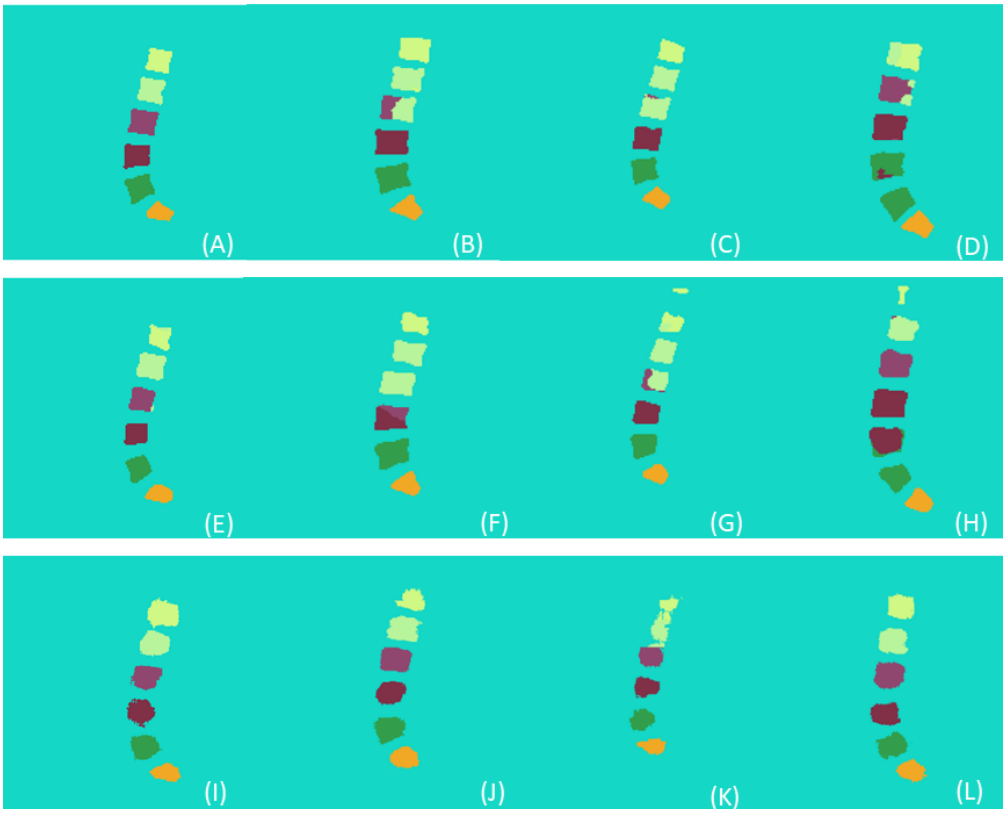

Figure 5.13: Qualitative comparison of semantic segmentation models.

Table 7: Quantitative Comparison of segmentation through different models.

S.NO	Models	Dice Coefficient	IOU
1	U-Net	**0.9902**	**0.8315**
2	SegNet	0.9871	0.7804
3	FCN_32	0.9790	0.6446

Table 8 shows the comparison of segmentation results of our proposed technique and other researchers work. Image types and the techniques used by the researchers are also shown in the table. Korez et al. [74] have performed the automatic segmentation on MRI scans and achieved the DC of 0.934±0.017 with their proposed 3D CNN architecture. Lu et al. [75] have used U-Net to segment the vertebral body and achieved IOU and DC of 0.93 and 0.91. In [76], researchers have used 3D hybrid level sets approach to segment the vertebral bodies and attained a DC of 0.86. Huang et al. [77] have developed spine explorer to segment and quantify the vertebrae and discs on lumbar spine MRI scans. U-Net is used for segmentation in spine explorer and it has attained the superior IOU of 0.947 in the table. FCN was used by [34] for segmentation with the DC value of 0.944±0.033. A multi-scale attention U-shaped network (MANet) is developed by [78] to segment the lumbar spine and they have achieved a DC Score of 0.92. We have achieved notably better DC as compared to the other researchers.

The range of IOU and DC is from 0 to 1, values close to 1 represent the best performance by the model. Bold values of Dice Coefficient and IOU show the highest values achieved by models.

Table 8: Comparison of segmentation results with different researchers.

S.No	Researchers	Models	Modalities	Dice Coefficient	IOU
1	Proposed Method	U-Net	MRI	**0.9902**	0.8315
2	Korez et al.	3D CNN	MRI	0.934±0.017	-
3	Lu et al.	U-Net	MRI	0.93	0.91
4	Hille et al	Hybrid Level Sets	MRI	0.86	-
5	Lessmann et al.	FCN	MRI	0.944±0.033	-
6	Huang et al.	U-Net	MRI	-	**0.947**
7	Li. et al	MANET	MRI	0.92	-

5.3.2 Lumbar Lordosis Assessment

We have used two ways to diagnose the lumbar lordosis. This first method is the lumbar lordosis assessment through region area where the area is correlated with the angles values to classify the disease while the other method is to assess the lumbar lordosis by finding the angle from the corners of the vertebrae. As we have used the same localization part in both methods therefore mAP has same values for both methods. The summary of all the results are shown in the table 9.

Table 9: Summary of results of lumbar lordosis assessment through region area and proposed methodology.

Method	Hypo		Normal		Hyper		mAp	Mean Error		Accuracy
	True	False	True	False	True	False		LLA	LSA	
Localization & Identification	6	0	11	8	21	5	0.975	-	-	74.5%
Overall Proposed Methodology	6	0	19	0	26	0	0.975	0.29	0.38	100%

CHAPTER 6: CONCLUSION & FUTURE WORK

6.1 Conclusion

In this paper, we have performed the YOLO annotations of lumbar Spine Composite Dataset [55], which consists of the mid-sagittal views of MRI scans. We have proposed the method to localize the lumbar spine and a sacrum using YOLOv5, and performed the calculations to compute the centroids of bounding boxes. The centroids are compared with ground truth centroids values which have very low mean error and high IOU in case of each lumbar and sacrum vertebra. Region area computed from the centroids decides the lumbar lordosis severity, i.e., sway back, normal or flat back, that will help the young doctors as a decision support system to diagnose the disease. The comparison of different semantic segmentation models is also presented in this paper, U-Net has the most promising results in segmenting the lumbar spine and sacrum with the DC and IOU of 0.99 and 0.83. SegNet and FCN_32 have the DC and IOU of 0.98, 0.78 and 0.97, 0.64 respectively. The angles, LLA and LSA are found by computing the corners of vertebra using Harris Corner Detector with a very less mean error and standard deviation. It is concluded from the experiments that image should be smoothed before finding the corners of vertebrae, unsmoothed images make corners detection a laborious task. For this purpose, a gaussian smoothing filter has been used to get the smoothed corners. LLA has 0.28˚ mean error which means it detects the lumbar lordosis, hypo, normal and hyper very efficiently.

6.2 Future Work

In the future, this work can be extended to diagnose the cervical, thoracic spine and pelvic region deformities. Object detectors like yolov5 and its new variants can be used to diagnose the spinal cord deformities. Also we can use different segmentation models for the spinal cord to calculate the cobb angles. Other direction may be used to investigate and develop a fully automated machine learning toolkit for spinal deformities to prevent invasive surgery methods.

REFERENCES

[1] Tang, Xiaoli. ”The role of artificial intelligence in medical imaging research.” BJR—Open 2.1 (2019): 20190031.

[2] pngkey.com Retrieved June 1, 2021 from https://www.pngkey.com/detail/u2w7r5o0e6t4a9a9\textunderscore structure-of-spine-human-spine-png/

[3] spineuniverse Retrieved June 1, 2021 from https://www.spineuniverse.com/anatomy/anatomical-planes-body

[4] healthline.com Retrieved June 1, 2021 from https://www.healthline.com/health/ct-scan-vs-mri#takeaway

[5] kids.frontiersin.org Retrieved June 1, 2021 from https://kids.frontiersin.org/articles/10.3389/frym.2019.00023#:~:text=MRI%20uses%20magnetic%20fields%20and,lots%20of%20signal%20to%20measure.

[6] Armstrong, Peter, and Stephen F. Keevil. "Magnetic resonance imaging--1: Basic principles of image production." *BMJ: British Medical Journal* 303.6793 (1991): 35.

[7] wiley.com Retrieved June 1, 2021 from https://onlinelibrary.wiley.com/doi/full/10.1002/jmri.23642

[8] Buxton, Richard B., et al. "Contrast in Rapid MR Imaging: T1− and T2-Weighted Imaging." *Journal of computer assisted tomography* 11.1 (1987): 7-16.

[9] Wolansky, Leo J., et al. "Magnetic resonance imaging protocols for cervical disc disease: What is your neighbor up to?." *Journal of Neuroimaging* 15.2 (2005): 183-187.

[10] radiologymasterclass.co.uk Retrieved June 1, 2021 from https://www.radiologymasterclass.co.uk/tutorials/mri/t1_and_t2_images

[11] myhealth.alberta.ca Retrieved June 1, 2021 from https://myhealth.alberta.ca/Health/aftercareinformation/pages/conditions.aspx?hwid=abq5157

[12] Mildenberger, Peter, Marco Eichelberg, and Eric Martin. "Introduction to the DICOM standard." *European radiology* 12.4 (2002): 920-927.

[13] Cooke Jr, Robert E., et al. "Picture archiving and communication system." U.S. Patent No. 6,574,629. 3 Jun. 2003.

[14] healthline.com Retrieved June 1, 2021 from https://www.healthline.com/health/lordosis#treatment

[15] medicalnewstoday.com Retrieved June 1, 2021 from https://www.medicalnewstoday.com/articles/324071#treatments

[16] spinemd.com Retrieved June 1, 2021 from https://www.spinemd.com/what-we-treat/spinal-deformities/flatback-syndrome/

[17] Lecron, Fabian, Mohammed Benjelloun, and Saïd Mahmoudi. "Fully automatic vertebra detection in x-ray images based on multi-class SVM." Medical Imaging 2012: Image Processing. Vol. 8314. International Society for Optics and Photonics, 2012.

[18] Glocker, Ben, et al. "Vertebrae localization in pathological spine CT via dense classification from sparse annotations." International conference on medical image computing and computer-assisted intervention. Springer, Berlin, Heidelberg, 2013.

[19] Koh, Jaehan, et al. "Automatic spinal canal detection in lumbar MR images in the sagittal view using dynamic programming." Computerized medical imaging and graphics 38.7 (2014): 569-579.

[20] Zuzanna, K., and S. Jacek. "Bones detection in the pelvic area on the basis of YOLO neural network." 19th International Conference Computational Problems of Electrical Engineering. 2018.

[21] McCouat, James, and Ben Glocker. "Vertebrae detection and localization in CT with two-stage CNNs and dense annotations." arXiv preprint arXiv:1910.05911 (2019).

[22] Zhong, Zhenxiao, and Jianzhi Deng. "Real-Time Detection based on Modified YOLO for Herniated Intervertebral Discs." Proceedings of the 2019 4th International Conference on Intelligent Information Processing. 2019.

[23] Yi, Jingru, et al. "Vertebra-Focused Landmark Detection for Scoliosis Assessment." 2020 IEEE 17th International Symposium on Biomedical Imaging (ISBI). IEEE, 2020

[24] Masuzawa, Naoto, et al. "Automatic Segmentation, Localization, and Identification of Vertebrae in 3D CT Images Using Cascaded Convolutional Neural Networks." International Conference on Medical Image Computing and Computer-Assisted Intervention. Springer, Cham, 2020.

[25] Sha, Gang, Junsheng Wu, and Bin Yu. "Detection of Spinal Fracture Lesions Based on Improved Yolo-tiny." 2020 IEEE International Conference on Advances in Electrical Engineering and Computer Applications (AEECA). IEEE, 2020.

[26] Pisov, Maxim, et al. "Keypoints Localization for Joint Vertebra Detection and Fracture Severity Quantification." International Conference on Medical Image Computing and Computer-Assisted Intervention. Springer, Cham, 2020.

[27] Ghosh, Subarna, and Vipin Chaudhary. "Supervised methods for detection and segmentation of tissues in clinical lumbar MRI." Computerized medical imaging and graphics 38.7 (2014): 639-649.

[28] Yang, Dong, et al. "Automatic vertebra labeling in large-scale 3D CT using deep image-to-image network with message passing and sparsity regularization." International conference on information processing in medical imaging. Springer, Cham, 2017

[29] Al Kafri, Ala S., et al. "Detecting the Disc Herniation in Segmented Lumbar Spine MR Image Using Centroid Distance Function." 2017 10th International Conference on Developments in eSystems Engineering (DeSE). IEEE, 2017.

[30] Janssens, Rens, Guodong Zeng, and Guoyan Zheng. "Fully automatic segmentation of lumbar vertebrae from CT images using cascaded 3D fully convolutional networks." 2018 IEEE 15th International Symposium on Biomedical Imaging (ISBI 2018). IEEE, 2018.

[31] Liao, Haofu, Addisu Mesfin, and Jiebo Luo. "Joint vertebrae identification and localization in spinal CT images by combining short-and long-range contextual information." IEEE transactions on medical imaging 37.5 (2018): 1266-1275.

[32] Sekuboyina, Anjany, et al. "VerSe: A Vertebrae Labelling and Segmentation Benchmark." arXiv preprint arXiv:2001.09193 (2020).

[33] Al-Kafri, Ala S., et al. "Boundary delineation of MRI images for lumbar spinal stenosis detection through semantic segmentation using deep neural networks." IEEE Access 7 (2019):43487-43501.

[34] Lessmann, Nikolas, et al. "Iterative fully convolutional neural networks for automatic vertebra segmentation and identification." Medical image analysis 53 (2019): 142-155.

[35] Mbarki, Wafa, et al. "Lumbar spine discs classification based on deep convolutional neural networks using axial view MRI." Interdisciplinary Neurosurgery 22 (2020): 100837.

[36] Natalia, Friska, et al. "Automated measurement of anteroposterior diameter and foraminal widths in MRI images for lumbar spinal stenosis diagnosis." PloS one 15.11 (2020): e0241309.

[37] Masood, Rao Farhat, et al. "DeepLearning based Vertebral Body Segmentation with Extraction of Spinal Measurements and Disorder Disease Classifcation", 2021, unpublished

[38] Kusuma, Bagus Adhi. "Determination of spinal curvature from scoliosis X-ray images using K-means and curve fitting for early detection of scoliosis disease." *2017 2nd International conferences on Information Technology, Information Systems and Electrical Engineering (ICITISEE)*. IEEE, 2017. [39] Pan, Yaling, et al. "Evaluation of a computer-

aided method for measuring the Cobb angle on chest X-rays." *European Spine Journal* 28.12 (2019): 3035-3043.

[40] Safari, A., et al. "A semi-automatic algorithm for estimating cobb angle." *Journal of biomedical physics & engineering* 9.3 (2019): 317.

[41] Chen, Bo, et al. "An automated and accurate spine curve analysis system." *IEEE Access* 7 (2019): 124596-124605.

[42] Kim, Kang Cheol, et al. "Automation of Spine Curve Assessment in Frontal Radiographs Using Deep Learning of Vertebral-Tilt Vector." *IEEE Access* 8 (2020): 84618-84630.

[43] Yao, Jianhua, et al. "Detection of vertebral body fractures based on cortical shell unwrapping." International Conference on Medical Image Computing and Computer-Assisted Intervention. Springer, Berlin, Heidelberg, 2012.

[44] Aslan, Melih S., et al. "A novel 3D segmentation of vertebral bones from volumetric CT images using graph cuts." International Symposium on Visual Computing. Springer, Berlin, Heidelberg, 2009.

[45] Ibragimov, Bulat, et al. "Shape representation for efficient landmark-based segmentation in 3-D." IEEE transactions on medical imaging 33.4 (2014): 861-874.

[46] Korez, Robert, et al. "A framework for automated spine and vertebrae interpolation-based detection and model-based segmentation." IEEE transactions on medical imaging 34.8 (2015): 1649-1662.

[47] Cai, Yunliang, et al. "Multi-modality vertebra recognition in arbitrary views using 3D deformable hierarchical model." IEEE transactions on medical imaging 34.8 (2015): 1676-1693.

[48] Zukić, Dženan, et al. "Robust detection and segmentation for diagnosis of vertebral diseases using routine MR images." Computer Graphics Forum. Vol. 33. No. 6. 2014.

[49] Yao, Jianhua, et al. "A multi-center milestone study of clinical vertebral CT segmentation." Computerized Medical Imaging and Graphics 49 (2016): 16-28.

[50] Wu, Hongbo, et al. "Automatic landmark estimation for adolescent idiopathic scoliosis assessment using BoostNet." International Conference on Medical Image Computing and Computer-Assisted Intervention. Springer, Cham, 2017.

[51] Pisov, Maxim, et al. "Keypoints Localization for Joint Vertebra Detection and Fracture Severity Quantification." International Conference on Medical Image Computing and Computer-Assisted Intervention. Springer, Cham, 2020.

[52] Liebl, Hans, et al. "A Computed Tomography Vertebral Segmentation Dataset with Anatomical Variations and Multi-Vendor Scanner Data." arXiv preprint arXiv:2103.06360 (2021).

[53] Burian, Egon, et al. "Lumbar muscle and vertebral bodies segmentation of chemical shift encoding-based water-fat MRI: the reference database myosegmentum spine." BMC musculoskeletal disorders 20.1 (2019): 1-7.

[54] Sudirman, Sud; Al Kafri, Ala; natalia, friska; Meidia, Hira; Afriliana, Nunik; Al-Rashdan, Wasfi; Bashtawi, Mohammad; Al-Jumaily, Mohammed (2019), "Lumbar Spine MRI Dataset", Mendeley Data, V2, doi: 10.17632/k57fr854j2.2

[55] Masood, Rao Farhat; Hassan, Taimur; Akram, Muhammad Usman; Taj, Imtiaz Ahmad; Qureshi, Muhammad Asad; Khan, Muhammad Babar (2021), "Composite Dataset of Lumbar Spine Mid-Sagittal Images with Annotations and Clinically Relevant Spinal Measurements", Mendeley Data, V2, doi: 10.17632/k3b363f3vz.2

[56] machinelearningmastery.com Retrieved August 30, 2021 from https://machinelearningmastery.com/object-recognition-with-deep-learning/

[57] Thuan, Do. "Evolution of YOLO algorithm and YOLOv5: the state-of-the-art object detection algorithm." (2021).

[58] Xu, Renjie, et al. "A Forest Fire Detection System Based on Ensemble Learning." Forests 12.2 (2021): 217.

[59] Wang, Chien-Yao, et al. "CSPNet: A new backbone that can enhance learning capability of CNN." Proceedings of the IEEE/CVF conference on computer vision and pattern recognition workshops. 2020.

[60] Wang, Kaixin, et al. "Panet: Few-shot image semantic segmentation with prototype alignment." Proceedings of the IEEE/CVF International Conference on Computer Vision. 2019.

[61] Chen, Yi-Lang. "Vertebral centroid measurement of lumbar lordosis compared with the Cobb technique." Spine 24.17 (1999): 1786.

[62] Yang, Benson P., Carina W. Yang, and Stephen L. Ondra. "A novel mathematical model of the sagittal spine." Spine 32.4 (2007): 466-470.

[63] Polly Jr, David W., et al. "Measurement of lumbar lordosis: evaluation of intraobserver, interobserver, and technique variability." Spine 21.13 (1996): 1530-1535.

[64] Heidler, Konrad, et al. "HED-UNet: Combined Segmentation and Edge Detection for Monitoring the Antarctic Coastline." *IEEE Transactions on Geoscience and Remote Sensing* (2021).

[65] Ronneberger, Olaf, Philipp Fischer, and Thomas Brox. "U-net: Convolutional networks for biomedical image segmentation." International Conference on Medical image computing and computer-assisted intervention. Springer, Cham, 2015.
[66] Xie, Saining, and Zhuowen Tu. "Holistically-nested edge detection." *Proceedings of the IEEE international conference on computer vision*. 2015.
[67] Harris, Chris, and Mike Stephens. "A combined corner and edge detector." Alvey vision conference. Vol. 15. No. 50. 1988.
[68] Carman, D. L., R. H. Browne, and J. G. Birch. "Measurement of scoliosis and kyphosis radiographs. Intraobserver and interobserver variation." The Journal of bone and joint surgery. American volume 72.3 (1990): 328-333.
[69] Lechner, Ricarda, et al. "Comparison of two-and three-dimensional measurement of the Cobb angle in scoliosis." International orthopaedics 41.5 (2017): 957-962.
[70] Cracknell, Jesse, Douglas M. Lawson, and John A. Taylor. "Intra-and inter-observer reliability of the Cobb measurement by chiropractic interns using digital evaluation methods." The Journal of the Canadian Chiropractic Association 59.3 (2015): 261.
[71] Badrinarayanan, Vijay, Alex Kendall, and Roberto Cipolla. "SegNet: A deep convolutional encoder-decoder architecture for image segmentation." IEEE transactions on pattern analysis and machine intelligence 39.12 (2017): 2481-2495.
[72] Long, Jonathan, Evan Shelhamer, and Trevor Darrell. "Fully convolutional networks for semantic segmentation." Proceedings of the IEEE conference on computer vision and pattern recognition. 2015.
[73] Saifi, Mohammad Yousuf, and Jimmy Singla. "Deep learning based framework for semantic segmentation of satellite images." 2020 Fourth International Conference on Computing Methodologies and Communication (ICCMC). IEEE, 2020.
[74] Korez, Robert, et al. "Model-based segmentation of vertebral bodies from MR images with 3D CNNs." International conference on medical image computing and computer-assisted intervention. Springer, Cham, 2016.
[75] Lu, Jen-Tang, et al. "Deep Spine: Automated lumbar vertebral segmentation, disc-level designation, and spinal stenosis grading using deep learning." Machine Learning for Healthcare Conference. PMLR, 2018.
[76] Hille, Georg, et al. "Vertebral body segmentation in wide range clinical routine spine MRI data." Computer methods and programs in biomedicine 155 (2018): 93-99.

[77] Huang, Jiawei, et al. "Spine Explorer: a deep learning based fully automated program for efficient and reliable quantifications of the vertebrae and discs on sagittal lumbar spine MR images." The Spine Journal 20.4 (2020): 590-599.
[78] Li, Haixing, et al. "Automatic lumbar spinal MRI image segmentation with a multi-scale attention network." Neural Computing and Applications (2021): 1-14.